MASTER THESIS

MODELLING LOCAL FIELD POTENTIALS IN THE SUBTHALAMIC NUCLEUS

Emiel J.E. Kleinsman

ELECTRICAL ENGINEERING, MATHEMATICS AND COMPUTER SCIENCE
BIOMEDICAL SIGNALS AND SYSTEMS

EXAMINATION COMMITTEE
Prof.dr.ir. P.J. Veltink
Dr.ir. T. Heida
Dr.ir. L.J. Bour
Dr. H.G.E. Meijer
K.J. van Dijk, MSc.

DOCUMENT NUMBER
BSS – 13-19

UNIVERSITY OF TWENTE.

28-08-2013

Abstract

Due to the increasing number of elderly people in the western world the amount of patients that suffer from Parkinson's disease is growing. This brain disorder causes a range of symptoms that seriously affect the quality of life for the patient. The cause of these symptoms is determined to be a pathological decrease of dopamine in the brains, which negatively affects the functioning of the basal ganglia (BG). This is a collection of nuclei in the brain that plays an important role in the control of the motoric system. The surgical ablation of one of these nuclei, the subthalamic nucleus (STN), has been a discovered to be an effective treatment for Parkinson's disease. In more recent history, this procedure has been replaced by electrically stimulating the STN, through a process known as deep brain stimulation (DBS) using an electrode that is implanted in the STN. Applying continuous high-frequency stimulation using this electrode has been found to have the same effect on Parkinsonian symptoms as the permanent destruction of the STN.

In addition to stimulation of the nucleus, this implanted electrode can also be used for the measurement of electrical activity in the STN in the form of local field potentials (LFPs). An LFP is the electric field that results from synchronous synaptic activity acting on neurons in a relatively large area around the measuring electrode. This synaptic input causes a local electrical current to flow through the cell membrane of the neuron. The current can be seen as a source with a particular polarity (depending on the type of synapse which determines the direction of the transmembrane current). An opposing current will flow through the rest of the membrane of the affected neuron (some parts of the cell conduct more current than others) to compensate for the current that is entering the cell at the site of the active synapse. This current is the so-called return current and constitutes a second, spatially more distributed source of opposite polarity.

Through different pathways that lead from other brain regions towards and through the BG the STN primarily receives input signals from the motor cortex (MC) and the globus pallidus externus (GPe). The input coming from the MC is excitatory while the projections from the GPe have an inhibitory effect on the STN. Previous research has shown that these two synaptic inputs project to different areas within the STN. Although there have been many studies into the general origin of LFPs and the functionality of the STN, the influence that different forms of mutual organizations of neurons and the type of synaptic inputs that these neurons receive have on the LFP that is generated in the STN is still largely unknown.

This study investigates the influence that these factors have on the measurable LFP by means of computer simulations. For these simulations, a computational model of a typical STN neuron was used. With this, the influence of groups of neurons that have different orientations relative to each other and to the measuring electrodes has been investigated. Simulated neurons were given various orientations and different positions in a three-dimensional array of electrodes and were provided with synaptic input. This synaptic input modelled projections from one of the main origins (MC or GPe) and was varied in amplitude throughout series of simulations. For each unique set of these parameters, the simulation resulted in a specific organization of the different current sources within the electrode array. The array was then used to measure the LFP that was generated by this constellation of sources, enabling the investigation of the effects of varying both neuronal

orientations and the influence of different types of input. The influence of the various factors has been assessed by examining the differences in the LFPs that are measured in both a single measuring electrode, as well as the effect they have on the LFPs' spatial distribution over the entire array.

As these simulations were performed with known parameters, comparing their results to corresponding *in vivo* measurements from earlier research enabled us to hypothesize on the organization of neurons in the STN around the projection areas from the MC and the GPe. The measurements and some of the simulations both clearly showed the sources that resulted from the different projection synapses, while the sources that were caused by the return currents had a much lower amplitude and had a relatively wide distribution over the area around the MC or GPe projection. Based on these observations and the parameters that constituted the simulations that best approximated the *in vivo* measurements, we believe that the neurons that receive input from the various projections do not have a particular parallel organization, but rather are individually orientated towards the projection area. This causes a concentrated source of synaptic activity, while the sources of the return current are much more distributed and therefore form a much less powerful source.

Samenvatting

Door de vergrijzing van de westerse populatie neemt de hoeveelheid patiënten die lijden aan de ziekte van Parkinson toe. Deze hersenaandoening veroorzaakt een scala aan symptomen die de kwaliteit van leven van de patiënt ernstig beïnvloeden. De oorzaak van deze symptomen is terug geleid tot een pathologische afname van dopamine in de hersenen, welke een negatief effect heeft op de werking van de basale ganglia (BG). Dit is een verzameling van kernen in de hersenen die een belangrijke rol spelen in het motorisch systeem. Het operatief verwijderen van één van deze kernen, de subthalamische nucleus (STN), is lang een behandeling voor de ziekte van Parkinson geweest. In de meer recente geschiedenis is deze ingreep vervangen door het elektrisch stimuleren van de STN, bekend als *deep brain stimulation* (DBS). Hierbij wordt een elektrode in de STN geïmplanteerd. Het toepassen van continue en hoogfrequente stimulatie door middel van deze elektrode heeft het zelfde effect op de symptomen van de patiënt als het permanent verwijderen van de STN.

Deze elektrode kan naast stimulatie van de nucleus ook toegepast worden voor het meten van elektrische activiteit in de STN, in de vorm van *local field potentials* (LFPs). Een LFP is het resultaat van synchrone synaptische activiteit die binnenkomt op neuronen in een relatief groot gebied rondom de meetelektrode De synaptische input in een neuron veroorzaakt een lokale elektrische stroom door het celmembraan. Deze stroom kan beschouwd worden als een bron met een bepaalde polariteit (afhankelijk van het type synaps en daarmee de richting van de transmembrane stroom). Een tegenovergestelde stroom vloeit door het membraan van de rest van het neuron en compenseert daarmee de transmembrane stroom ten gevolge van het synaps. Deze zogenaamde *return current* vormt een tweede, spatieel meer gedistribueerde bron met tegengestelde polariteit.

Via verschillende paden die vanuit andere delen van de hersenen richting en door de BG lopen ontvangt de STN voornamelijk signalen vanuit de motor cortex (MC) en de globus pallidus externus (GPe). Hierbij is de input vanuit de MC excitatoir is terwijl de GPe juist een inhibitoir effect heeft op de STN. Uit eerder onderzoek is gebleken dat deze twee synaptische inputs op verschillende posities binnen de STN geprojecteerd worden. Hoewel er veel onderzoek gedaan is naar de algemene opbouw van LFPs en naar de functie van de STN, is de invloed die mogelijke onderlinge organisatie van neuronen en de eigenschappen van de synaptische input die deze neuronen ontvangen hebben op het gegenereerde LFP in de STN nog steeds grotendeels onbekend.

In deze studie is de invloed van deze factoren op het meetbare LFP onderzocht door middel van computersimulaties. Voor deze simulaties is een computationeel model van een typisch STN neuron gebruikt. Hiermee is de invloed van neuronen die in verschillende oriëntaties ten opzichte van elkaar en de meetelektroden geplaatst zijn onderzocht. Gesimuleerde neuronen zijn in een drie dimensionaal array van 320 elektroden te plaatsen en voorzien van synaptische input. Deze synaptische input is gemodelleerd op projecties afkomstig van de MC of de GPe terwijl de amplitude een variabele parameter vormde. Voor iedere unieke set van deze parameters resulteerde de simulatie ervan in een specifieke organisatie van de verschillende stroombronnen binnen de elektrodearray. Dit driedimensionale array werd vervolgens gebruikt om het LFP dat door deze constellatie van stroombronnen werd opgewekt te meten, waardoor het mogelijk werd om de effecten van variatie in zowel de oriëntatie als de verschillende vormen van synaptische input te

bestuderen. Deze effecten zijn beoordeeld aan de hand van LFP metingen op zowel een enkele elektrode en de meting van de ruimtelijke verdeling van het LFP door gebruik te maken van alle 320 elektroden.

Door de uitkomsten van deze simulaties, die uitgevoerd zijn met bekende parameters, te vergelijken met overeenkomstige *in vivo* metingen uit eerder onderzoek, werd het mogelijk uitspraken te doen over de waarschijnlijke organisatie van neuronen in de STN rondom de regio's waar synaptische input vanuit de MC en de GPe binnenkomt. De *in vivo* metingen en aantal van de simulaties tonen duidelijke bronnen ten gevolge van de verschillende projectiesynapsen, terwijl bronnen van de *return current* zich met een veel lagere amplitude en een grote ruimtelijke verdeling in het gebied rondom deze projectie lijken te bevinden. Op basis van deze observaties en de parameters van de simulaties die de *in vivo* metingen het beste benaderden, geloven wij dat er bij de neuronen die synaptische input ontvangen van projecties vanuit de MC of GPe geen sprake is van een onderlinge parallelle structuur, maar dat lengte as van elk van deze neuronen individueel naar het gebied van projectie gericht is. Hierdoor ontstaat een geconcentreerde bron van synaptische activiteit ten gevolge van de projecties, terwijl de bronnen van de *return current* veel meer verspreid liggen en daardoor een veel minder sterke bron vormen.

Table of Contents

1. Introduction

1.1 Parkinson's Disease

1.1.1 Introduction to Parkinson's disease

Parkinson's disease (PD) is a progressive neurodegenerative disease that mainly affects the elderly, second in frequency of appearance only to Alzheimer's disease. As the medical care grows better and with the baby-boomers reaching their golden years, the number of people within the western population that run the risk of developing PD increases over time. It is estimated that in 2030, the 10 most populated nations in the world will have between 8.7 and 9.3 million PD patients **(*Dorsey et al, 2007*)**. Therefore research into this condition grows ever more important.

The disease was first described in 1817 in "An essay on the shaking palsy" by the man whose name the disease would later bear, James Parkinson. As his description shows, Parkinson mainly saw the characteristic tremor that is most common in PD patients. Later in the 19th century, Jean-Martin Charcot added other manifestations of PD to the list of symptoms, such as slowness of movement **(*Lees, 2007*)**.

Our modern definition of PD has four important symptoms, gathered in the acronym 'TRAP', or Tremor at rest, Rigidity, Akinesia (or bradykinesia) and Postural instability. While these are the most commonly seen symptoms, PD is also associated with symptoms that are not motor related such as autonomic disfunctionality, sensory and sleep abnormalities and disorders that are of a cognitive or neurobehavioral nature. This makes PD a disease with a wide range of debilitating effects **(*Jankovic, 2008; Hammond, 2007*)**.

1.1.2 The cause Parkinson's disease

Finding the exact cause of PD is still very much a work in progress. Although the disease is known since the beginning of the 19th century, it was not until the 20th century that the loss of cells in the substantia nigra pars compacta (SNc) and changes in dopamine concentrations were related to PD. In the current understanding of the disease, the reason for the degeneration of dopaminergic neurons in the SNc remains unclear. It is, however, apparent that a decrease in dopamine levels in the brain plays a major role and that cell death in the SNc is hallmark for PD. In case of PD, this brain region is known to contain 50-70% less neurons at the time of death compared to a healthy SNc **(*Davie, 2008*)**.

The SNc is a part of the midbrain that projects onto the striatum. The latter receives (glutamatergic) input from the thalamus and from the cerebral cortex and in turn projects onto the system formed by the globus pallidus internus (GPi) and externus (GPe) and the SNc **(*Hammond, 2007*)**. It is therefore the main entrance for information into a constellation of nuclei in the brain known as the basal ganglia (BG).

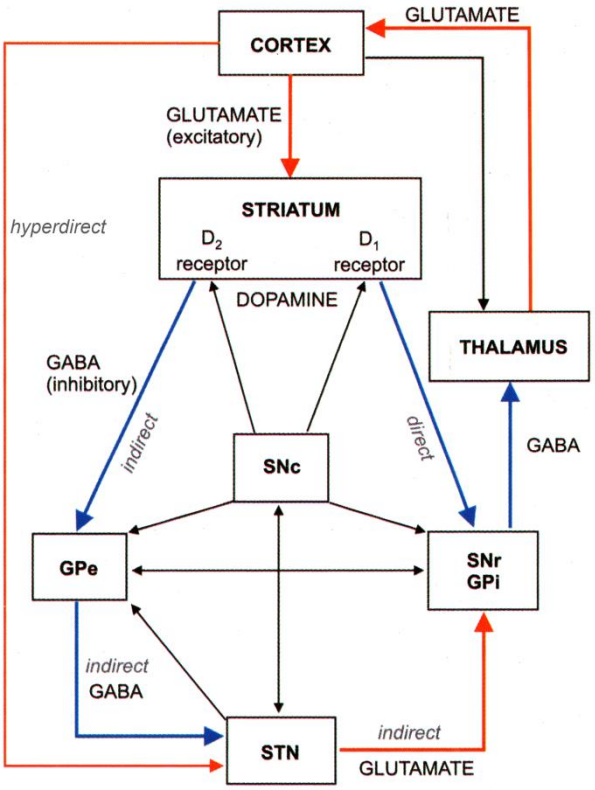

Figure 1.1: ***Schematic view of the cortico-basal ganglia thalamocortical circuit, showing the three main pathways that conduct motor related signal into and out of the basal ganglia. The direct and indirect and hyperdirect pathways are indicated. The hyperdirect pathway is formed by the excitatory projections directly from the cortex to the STN, shown on the left (*****Nambu et al, 2002*****). Red arrows indicate excitatory connections and blue arrows inhibitory connections. (Figure modified from (*****Marani et al, 2008*****))***

1.2 Basal Ganglia

The BG is a collection of nuclei that have tight interconnections and it is a major link in the motor control loop in the brain. During normal operation the output nuclei of the basal ganglia, the substantia nigra pars reticulata (SNr) and the GPi, will continuously inhibit the thalamocortical connection. Various types of input into the BG activate three different internal pathways between the different nuclei (i.e. the indirect, direct and hyperdirect pathways, refer to figure 1.1), which in turn leads to either extra inhibition or disinhibition of this thalamocortical connection. The effect of the received input depends on the distribution of activation over the three different pathways. In the case of an inhibiting effect on the output nuclei, any on-going movement will be reduced, while disinhibition enables the selection, initiation and modulation of new movements **(*Joel and Weiner, 1996*)**.

The reduction in dopamine that is caused by PD negatively affects the communication between the SNr and the striatum, causing a pathologic imbalance between activation of the direct and indirect pathways. Cell loss within the SNc further cripples normal operation of the BG **(*Hammond, 2007; Davie, 2008*)**. In the Parkinsonian BG, synchronization between nuclei causing abnormal oscillations

in the beta-band (10-30 Hz) has been linked to pathological behaviour **(*Bevan et al, 2002; Brown, 2003; Brown, 2007; Weinberger and Dostrovsky, 2011*)**.

Besides the striatum, the BG contains another nucleus that receives input signals from outside of the BG, the subthalamic nucleus (STN). Over time and through animal and traumatic lesion studies, this nucleus has been found to play a major role in the possible cause, pathology and treatment of PD.

1.3 The Subthalamic Nucleus

Since the importance of the STN became apparent, a lot of research has been done to find out more about the exact function and modes of operation of this nucleus. Most of this research has been done in rat, because of the need for living material and *in vivo* measurements which rule out human subjects.

The STN is responsible for excitatory projections to the output nuclei of the BG in the indirect and hyperdirect pathways, provoking inhibition of the thalamocortical structure and is therefore modulating the slowing or stopping of movement **(*Parent and Hazrati, 1995*)**.

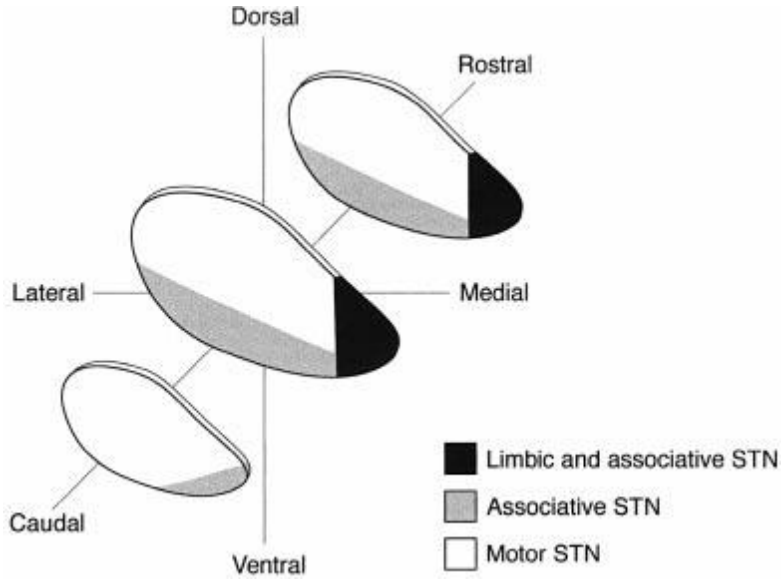

Figure 1.2: ***Illustration of the intrinsic organization of the primate STN, divided into three functional regions (Figure modified from (*****Hamani, 2003*****))***

As can be seen in figure 1.2, the STN is divided into three sub-regions that are responsible for different tasks. Each region is defined by the functional circuit of the brain it is connected to (motor, associative and limbic). The main focus of this study will be on the motor region as this is where Parkinsonian pathology is encountered **(*Hamani, 2003*)**.

Input

The motor region of the STN receives mainly two types of input signals, from the motor cortex (MC) through the hyperdirect pathway and from the GPe through the indirect pathway, as can be seen in figure 1.1. The signals that are received from the MC are excitatory and are relayed onto the STN neurons mainly through AMPA and NMDA synapses. The projections that originate in the GPe have an inhibitory nature and mainly use synapses of the $GABA_A$ type **(*Götz et al, 1997; Clarke and Bolam, 1998; Magill et al, 2004*)**. Although both of these types of input are limited to the same motor region of the STN, it is hypothesized that they have individual projection areas within that region as is illustrated in figure 1.3 **(*Van Dijk et al, 2012*)**.

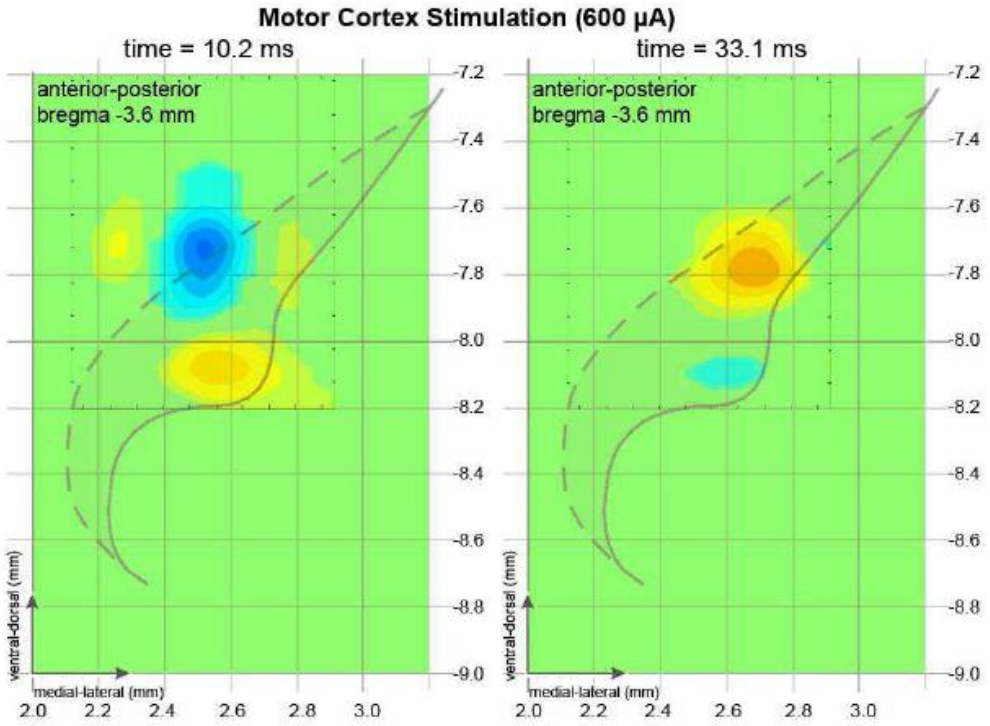

Figure 1.3: ***Results from measurements performed in the rat STN by (Van Dijk et al, 2012). These plots show the current source density (CSD) – or the spatial distribution of current sources – in a cross section of the STN for different types of projected input. Left) Sources due to projections from the MC; Right) Sources due to projections from the GPe. It can be seen that the positions of the sources are different for each type of input.***

Output

The neurons that are present in the motor related region of the STN mainly project towards the output nuclei and are located in the caudal third and in the dorsal aspect of the lateral portion of the rostral two-thirds of the STN (see figure 1.2) **(*Hamani, 2004*)**.

Through colouring studies in primates, five different types of projecting neurons have been identified, each of which have a distinct set of projection targets **(*Sato, 2000*)**. Other classes of neurons like interneurons are found in the STN as well, but these tend to stay within the borders of the nucleus and therefore mainly serve the internal communication **(*Lévesque and Parent, 2005*)**.

The morphology of these projection neurons has been studied and compared to other regions of the brain, such as the cerebral cortex. While the latter has a very clear and ordered structure of parallel placed pyramidal cells, the neurons in the STN tend to form a seemingly less organized network **(*Sato, 2000; Lévesque and Parent, 2005*)**.

1.4 Deep Brain Stimulation

1.4.1 Treatments for Parkinson's disease

There are two main treatments for PD, medication and surgery. With modern medical knowledge and technology, PD still remains an incurable disease. Therefore, all forms of treatment are currently aimed at the reduction of symptoms.

Medication

After diagnosing a patient with PD, the first approach is to counteract the pathological dopamine reduction. This is most commonly done by administering levodopa. This drug contains L-DOPA, which is the precursor of dopamine **(*Mouradian et al, 1990; Pahwa and Lyons, 2009; Davie, 2008; Jankovic, 2008*)**.

Although treatment with levodopa does decrease the severity of the symptoms, its effect is not persistent. After a certain period (the duration of which is still topic of debate, but lays in the order of 5-10 years) the patient will again start experiencing PD symptoms. To counteract this, the patient's dosage of levodopa is increased. This, however, is again only a temporary solution as high doses of levodopa are known to cause severe side effects such as dyskinesia and motor fluctuations in which patients cycle between periods of good mobility (the so called "on" periods) and impaired mobility ("off" periods). As this level of severity is reached, medication is no longer adequate and the only alternative is surgery **(*Mouradian et al, 1990; Pahwa and Lyons, 2009; Stocchi, 2006; Davie, 2008*; *Jankovic, 2008*)**.

Deep Brain Stimulation

The use of surgery in the treatment of Parkinson's disease has seen two stages, ablative surgery and later the implantation of a stimulation electrode in a specific target area of the brain, or deep brain stimulation (DBS).

When the BG were pinpointed as the major area of interest in PD pathology, certain nuclei within this structure were targeted for ablative surgery. While this proved to be quite a successful approach, ablation is a very invasive and non-reversible operation.

DBS has been found to have the same effect on brain structures as one would have from lesioning that structure. DBS is relatively young as a treatment for Parkinson's disease, as the American Food

and Drug Administration (FDA) approved its application against Parkinson's disease in 2002 **(*U.S. Department of Health and Human Services*)**. Although the underlying principles and mechanisms are not yet understood, there are several theories. These vary from inhibiting or exciting the entire STN to manipulating cortical projections that enter the STN **(*McIntyre et al, 2004; Gradinaru and Morgi, 2009*)**. Regardless of the precise mechanism involved, it is presumed that DBS counteracts the pathological synchronization within the BG **(*Hammond et al, 2007*)**.

Figure 1.4: ***Illustration of a patient with bilaterally implanted electrodes and subdural connections to two stimulator units implanted in the chest***

Nowadays, DBS has all but replaced ablative surgery. Its success can mainly be attributed to it being fully reversible. That is, as opposed to ablative surgery, turning off the stimulator effectively returns the target structure to its preoperative state **(*Deep-Brain Stimulation for Parkinson's Disease Study Group, 2001*)**.

A downside of DBS is the occurrence of side effects of the stimulation. Due to electrode size and a certain level of inaccuracy during electrode placement inherent to the current state of medical technology, not all current that is sent into the electrode affects the STN. Other nearby regions are also stimulated, which leads to unintended activation **(*Temel et al, 2006*)**. The physical expression of this stimulation outside of the target area is one of the key pointers that are used to assess electrode positioning and optimal stimulus strength during the implantation procedure **(*Hemm and Wårdell, 2010*)**.

As the correct positioning of the electrode is paramount, two different approaches to finding the correct stimulation site for the electrode are taken simultaneously. The first is imaging. MRI is used to locate the STN in the patient's brain before the operation. These images are also used to determine the best route from the scalp to the target area, navigating around major structures in the brain and avoiding blood vessels. However, due to large amounts of metal in the rig that is placed on the head of the patient to control the implantation, MRI suffers from artefacts that prevent locating the STN with adequate precision. Therefore, a more precise approach is required. The second approach to pinpointing the target area provides this accuracy and involves finding pathological signals that originate exclusively in the target.

Several of the nuclei within the BG are involved in intranuclear feedback loops. In the pathological BG a synchronisation of firing patterns emerges among these nuclei, causing synchronized oscillations in the beta-band (i.e. between 12-30 Hz) which are hallmark for Parkinson's disease **(*Bevan et al, 2002; Brown, 2003; Hammond, 2007; Brown, 2007*)**. The main source of this beta-band activity in the BG is the subthalamic nucleus (STN). During surgery this region can therefore be located by probing for these oscillations. Micro electrode recordings (MER) are made at several sites in and around the target area that was selected on the MRI. These are then checked for signals that are the result of tell-tale oscillatory behaviour in the STN. When these MERs have provided a site that clearly lies within the target area, that electrode is replaced with the DBS electrode **(*Chen et al, 2005; Rezai et al, 2006*)**.

A problem with this approach is that each insertion of an electrode introduces a risk of causing a bleeding in the brain. It is therefore preferable to avoid inserting multiple electrodes, and to be able to implant a single electrode that can be used for both locating the target area and the stimulation itself. Currently, research is being done to enable such an approach. To this end a new electrode has been designed that provides the possibility of directionally selective measuring and stimulation **(*Martens et al, 2010*)**. With such an electrode, directional measurements of the local field potentials (LFP) can be made. By analysing the LFPs that are recorded at the different electrode contacts the optimal stimulation direction is determined that will ensure that the injected current reaches the target area.

1.5 Local Field Potentials

Electrical signals in the brain come in roughly two types: the activity of individual cells and the cumulative signals from large areas in the brain that contain contributions of millions of cells. The former can be measured by placing a very small electrode inside or right up against a single cell (an MER). Measuring the cumulative activity of large numbers of cells is done by implanting a relatively large electrode in the area of interest. The signal that is recorded from this electrode then contains not only the small contributions from individual cells that happen to be in the direct vicinity of the electrode, but also the local electric field which consists of many signals from a large region around the electrode.

The electrode that is implanted for DBS is of the second, larger type. At the moment, measurements with this electrode are only done during implantation, as the measured signals can be used to assess whether the electrode is in the target area by checking them for characteristic beta-band (12-30 Hz) activity **(*Chen et al, 2005; Rezai et al, 2006*)**. During normal use (i.e. post-operation), the electrode is only used for stimulation and is connected to a stimulator unit that is implanted in the chest. However, the implanted electrode that is currently used for DBS (i.e. only stimulation) itself is perfectly capable of measuring the LFP.

The electrical signals that can be measured with an electrode like this mainly result from synaptic activity between neurons **(*Buzsáki, 2012*)**. When a synapse is activated, a small amount of

neurotransmitter is sent into the space between the two neurons, where it causes ligand gated ion channels in the postsynaptic neuron to open. These open channels then enable certain ions (each type with its own electrical charge, negative or positive) to flow through the cell membrane, causing a net electrical current into or out of the postsynaptic neuron at the location of the synapse **(*Kandel et al, 2000*)**. As the current enters or leaves the neuron at a specific location, the potential of the area in the direct vicinity will become different from that of the surrounding area, creating an electric field. As synapses are mostly found attached to the dendritic tree of an STN neuron, this is the main location of the LFP source. A second source is formed by the so called 'return current', which represents the current that leaves the cell to compensate for the current that was injected at the synapses. This current source is less local than the synaptic current, as it is distributed over the soma and all dendritic elements that did not receive the synaptic current **(*Pettersen et al, 2010; Buzsáki, 2012*)**.

Figure 1.5: ***Illustration of the presynaptic axon and the postsynaptic dendrite, synaptic cleft and emission of neurotransmitter therein due to activation of the synapse***

Whether the net current through the neuron membrane is excitatory or inhibitory depends on its direction and polarisation. The former is the case when the neurons membrane potential is brought closer towards its firing threshold and therefore leads to a slight depolarisation (an excitatory post synaptic potential, or EPSP), while the latter is true if current brings the membrane potential farther away from the firing threshold, causing a slight hyperpolarisation of the cell (an inhibitory post synaptic potential, or IPSP). This synaptic activity is called subthreshold as long as the sum of the received EPSPs and IPSPs in the postsynaptic neuron does not cause the neurons membrane potential to reach its firing threshold. However, if this threshold is reached, the neuron will fire an action potential (AP) **(*Kandel et al, 2000*)**.

The main differences between an AP and subthreshold synaptic activity - from a measuring perspective - are that the former is traveling along the neurons axon (i.e. is non-stationary) and is presumed to represent the output of the observed area while the latter represents its input and remains at a fixed location (i.e. the resulting current source is spatially fixed at the position of the synapse it originates from), evoking a potential field that is stationary. Also, APs are relatively fast events compared to postsynaptic potentials. During the measurement of LFPs, APs - or spikes - are filtered out of the data by only considering frequencies between 0 and 300 Hz, while the signals resulting from synaptic activity remain as they are much slower than the APs **(*Buzsáki, 2012; Pettersen et al, 2010*)**.

The current and with that the electric field that originates at a single synapse, however, is very small. Only if many synapses in the area around the measuring electrode are activated simultaneously, a measurable field is produced. Such synchronised fields can be measured from hundreds of micrometres up to some millimetres away from their source **(*Holt and Koch, 1999; Kajikawa and Schroeder, 2011; Buzsáki, 2012; Pettersen et al, 2010*)**.

The distance from the source over which this neuronal activity still affects the LFP at a certain position varies with different local tissue configurations. For instance, because neurons in the cortex (i.e. pyramidal cells) are positioned in a parallel, vertical alignment, conductivity in the vertical direction is very high. This enables LFPs to travel long distances in that direction, while the much lower horizontal conductivity causes the LFP to be attenuated over a much shorter range **(*Lindén et al, 2011; Kajikawa and Schroeder, 2011; Pettersen, 2008; Buzsáki, 2012*)**.

Computational Modelling Studies

Research into LFPs using computational modelling has already been done quite extensively for neurons in the cerebral cortex. This brain region generates relatively strong LFPs, since the local neurons are mostly positioned in a parallel fashion. This makes for sources that are very neatly ordered in layers, which result in clear LFPs when measured by an electrode array that is perpendicular to these layers **(*Buzsáki, 2012*)**.

A computational modelling study into such LFPs has been done by **(*Pettersen et al, 2008*)**. A simulation was made using NEURON, a simulation environment that is very able to simulate biological neurons and networks (instead of only working with, for example, very simple integrate-and-fire neuron models). **(*Hines, 1993*)**. In that study, a column of cortical neurons (i.e. pyramidal cells) was given a synaptic stimulus, causing synchronous currents across the cell membranes to generate an LFP. This LFP was measured using a simulated electrode array that was placed in the centre of the column. This resulted in LFP measurements at several heights, relative to the soma's and synaptic activity (illustrated in figure 1.6).

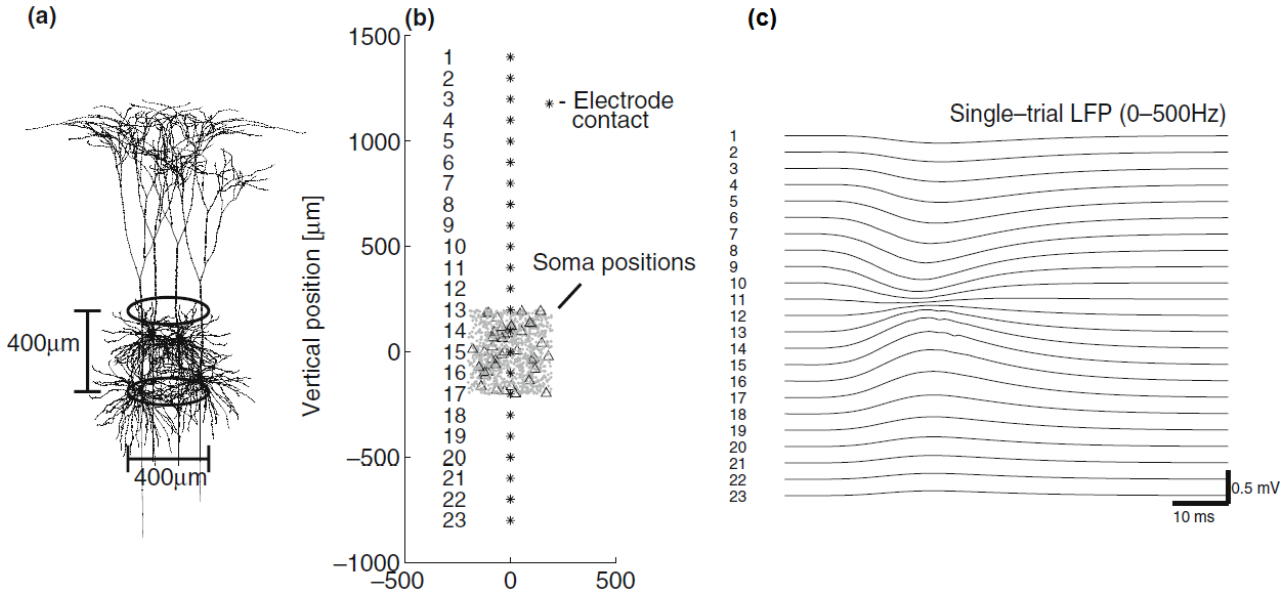

Figure 1.6: ***Simulation setup and example of resulting LFP from (*****Pettersen et al, 2008*****). a) The soma's of the parallel neurons are placed within the boundaries of an imaginary cylinder; b) An array of 23 electrodes placed coaxially to this cylinder, parallel to the present neurons; c) The LFP that is measured at the electrode array, low-pass filtered at 500 Hz in order to exclude action potentials from the signal***

However, since an LFP depends heavily on the spatial organization of neurons and synaptic input, the results of this or any other study of LFPs in the cortex cannot simply be said to apply to the STN, as this parallel organization of the neurons within the cortex is very characteristic and is not found in a region such as the STN.

1.6 Local Field Potentials in the Subthalamic Nucleus

Although morphologies of neurons in the STN have been mapped through colouring and tracing studies **(*Sato, 2002; Lévesque and Parent, 2005*)**, it is not clear what effect the morphological properties of the neuronal structure in the area surrounding the electrode contact have on the LFP that is recorded in the STN.

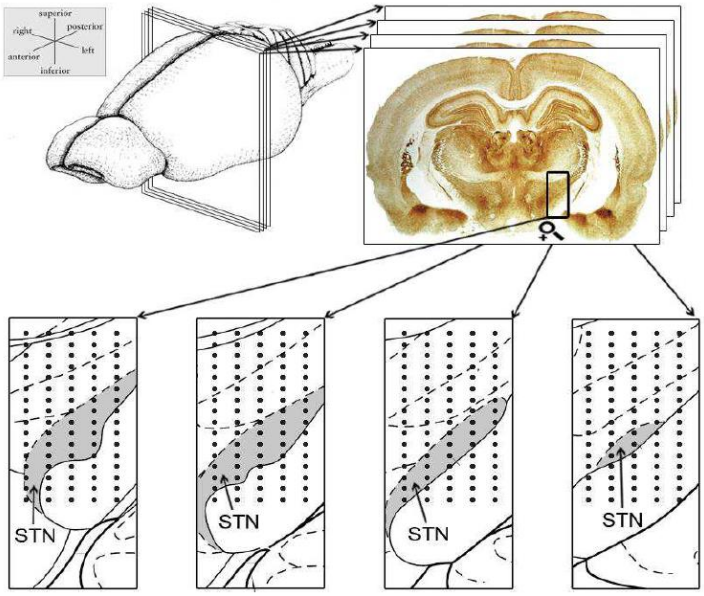

Figure 1.7: ***(Adapted from (Van Dijk et al, 2012)) During their experiments, Van Dijk et al inserted electrodes in live rat brains in order to record (amongst others things) LFPs at a total of 320 locations in and around the rat STN***

In the study of **(*Van Dijk et al, 2012*)**, electrodes are inserted in and near the rat STN as shown in figure 1.7. Evoked LFPs were measured by introducing a single stimulus to the motor cortex and recording the resulting LFPs in the STN using an array of electrodes. These MC evoked LFPs have a very specific shape, as was first determined by **(*Magill, 2004*)**. **(*Van Dijk et al, 2012*)** related this typical LFP to two individual current sources within the motor related area of the STN as a result of the stimulation, located at significantly different positions. This LFP, shown in figure 1.8, contains four specific elements which are described in table 1.1.

The same characteristic shape of the evoked LFP as is described by **(Magill, 2004)** was recorded by **(Van Dijk et al, 2012)** in several rats. Although the different elements (i.e. peaks N1..P2) were also found by this study, the definition of these peaks was not as strong as was reported by Magill (illustrated in figure 1.9).

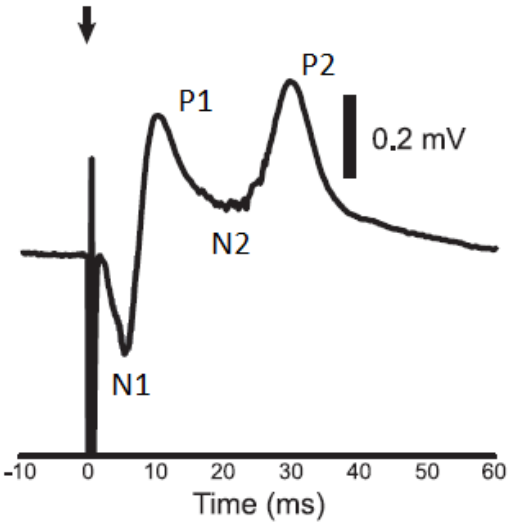

Figure 1.8: ***The LFP as was recorded by Magill in the rat STN following a stimulus in the ipsilateral motor cortex, showing the four characteristic elements in such an LFP. The moment of stimulation is indicated by the arrow. (Figure modified from (*****Magill et al, 2004*****))***

Table 1.1: ***Description of the four characteristic elements of the evoked LFPs measured by (Magill, 2004) and (Van Dijk et al, 2012)***

N_1	Negative deflection that occurs around 9.5 ms after the stimulus in the MC and which is the result of direct excitation of the STN by the MC (through the *hyperdirect pathway, shown in figure 1.1*)
P_1	Positive deflection occurring 14.5 ms post-stimulus. P_1 is believed to be the result of the STN, after being activated by the MC, exciting the GPe. The activated GPe then inhibits the STN
N_2	Negative deflection that follows P1, is suspected to be the result of the MC stimulus following the *indirect pathway*, inhibiting the GPe which leads to a disinhibition of the STN
P_2	Positive deflection P_2 that occurs 32.2 ms after the MC stimulus is given. The origin of this peak is not yet understood. It is expected to also be the result of projections from the GPe onto the STN **(*Zwartjes et al, 2013*)**.

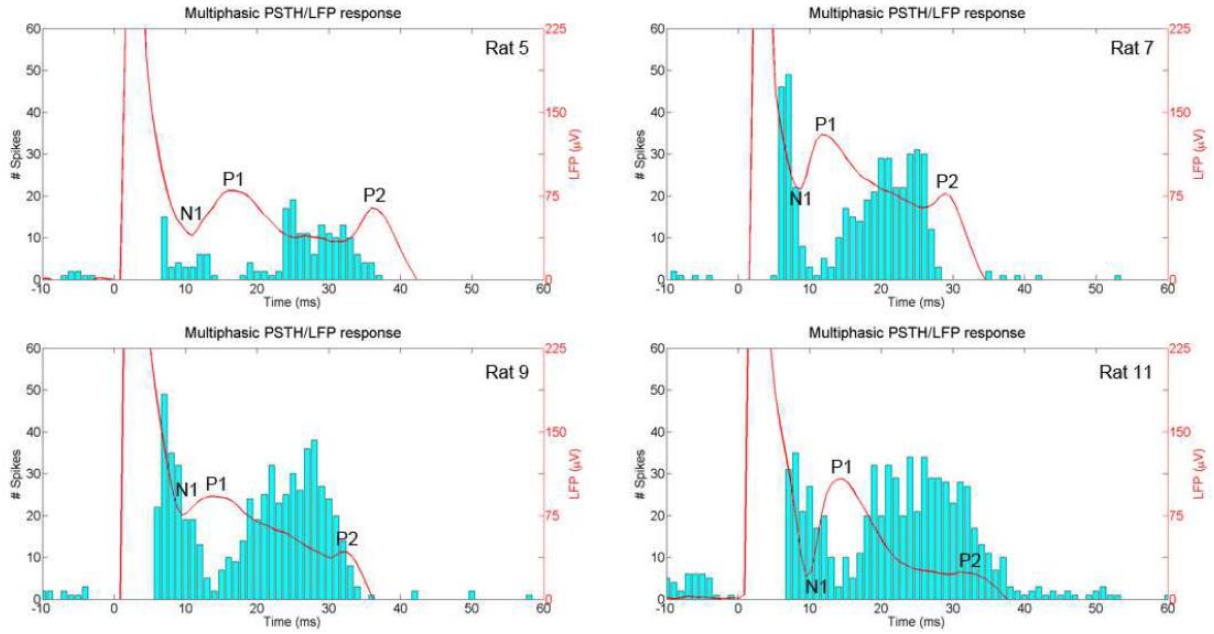

Figure 1.9: ***The characteristic evoked LFPs, measured by (*****Van Dijk et al, 2012*****) in several rat STNs. The LFPs are plotted as a red line, while the blue bars show the amount of APs that were recorded throughout the experiment. The peak at t=0 is a artefact that is caused by the stimulation that is delivered in the MC, which evokes the recorded LFP***

An LFP is the result of synchronous activity in multiple cells and the contribution of a single neuron is usually negligible. Also, it is unlikely that the LFPs recorded by Magill and Van Dijk are the result of completely randomly distributed and orientated neurons, as complete randomness in position and orientation would cause the overall LFP to be very low, due to opposing signals cancelling each other out **(*Buzsáki, 2012*)**. Based on these two considerations it may be hypothesized that there must be a certain organization of the neurons within the STN. However, the effects of different regionally common orientations of neurons, synaptic strengths and the type of active synapses on the LFP that is produced in the STN are not yet clear.

1.7 Research Question

The general information obtained from **(Buzsáki et al, 2012)** and computational model studies such as performed by **(Pettersen et al, 2008)** show some preliminary insights into the generation of an LFP and the influence of several factors thereupon. However, by comparing the STN to the cortex, some clear differences are observed. Mainly the organization of neurons within both structures is very different. Whereas the neurons that are found in the cortex have a very characteristic parallel organization, such structures have not been observed in the STN.

However, a better understanding of the effects that the organization of neurons amongst each other and other factors such as the type and amount of synaptic input due to different projections from other brain regions have on an LFP that is recorded in the STN is an important step towards a better understanding of the subthalamic nucleus. Such knowledge will contribute to a better understanding of the role of the STN within the basal ganglia in case of Parkinson's disease and can therefore lead to a better understanding of Parkinson's disease itself. Furthermore, by being able to gain knowledge about the neuronal structure that surrounds the implanted electrode and the activity therein through analysing the recorded LFP, sources of pathological activity may be localized without the need for inserting multiple MER probes. These areas can then be targeted through DBS that is aimed at the pathological region **(Martens, 2010)**. This, in turn, will make it possible to create closed-loop systems that can determine the required stimulation (with parameters such as intensity and direction of the stimulation), based on the LFP that is recorded at that moment, thereby eliminating the necessity for medical personnel for each 'tune-up' of the patient's stimulation.

The goal of this study is to investigate the effects of these different factors (i.e. the orientation of clusters of neurons that receive synaptic input, the amount of synaptic activity, the type of synapses that is active and the location of these cells and synapses relative to the recording electrode) on the LFP that can be measured in the STN. For this a series of computational modelling simulations will be performed, focussing on each of the factors individually.

Each simulation will contain a cluster of neurons that is placed inside a three dimensional array of 320 electrodes and that share a specific set of parameters, compiled from the variables that represent the aforementioned factors. That is, all neurons in such a cluster have the same orientation and general position relative to the electrode array. They also will receive the same type of synaptic input. Using this approach, each single set of parameters is simulated. Using linear superposition the LFPs that result from these simulations are then combined to investigate what the effects on the generated LFP are under such combined conditions, such as the presence of neurons of multiple orientations and whether or not different projections (i.e. coming from either the MC or the GPe) are located at individual positions or share the same location.

The results of this computational modelling study will be investigated qualitatively by comparing the amplitudes of the recorded LFPs on a single electrode for different sets of parameters and by considering the effects that can be observed in the spatial distribution of the LFP, measured throughout the simulated electrode array. To assess the accuracy of the model, its predictive qualities and its shortcomings, the simulated LFPs are compared to *in vivo* evoked potential measurements done in rats **(Magill, 2004; Van Dijk et al, 2012)**.

2. Methods

The simulations in this study are performed within NEURON, a computational simulation environment **(*Hines, 1993; Carnevale and Hines, 2006*)**. In order to simulate the LFP that is generated due to synaptic projection activity in the STN from the MC and the GPe, a model of a typical STN neuron is used as a template for all simulated cells. This model has been adapted to better suit the requirements for this study. The complete model is described in chapter 2.1. The different model parameters that were varied in this study are described in chapter 2.2. Finally, the data analyses methods are described in chapter 2.3.

2.1 Modelling

2.1.1 Cell Model

The model that is used for the dynamic behaviour of the STN neurons in these simulations is the one that was proposed by **(*Gillies and Willshaw, 2006*)**, with the three dimensional structure as was introduced for it by **(*Gillies and Sterrat, 2012*)**, illustrated in figure 2.1. This model is a computational multi-compartment model of the rat subthalamic projection neuron and it incorporates a specific set of modelled ion channels to create an active membrane. The properties of this active membrane and the other model parameters that are defined by **(*Gillies and Willshaw, 2006*)** make the cell exhibit activity patterns that are characteristic for an STN neuron.

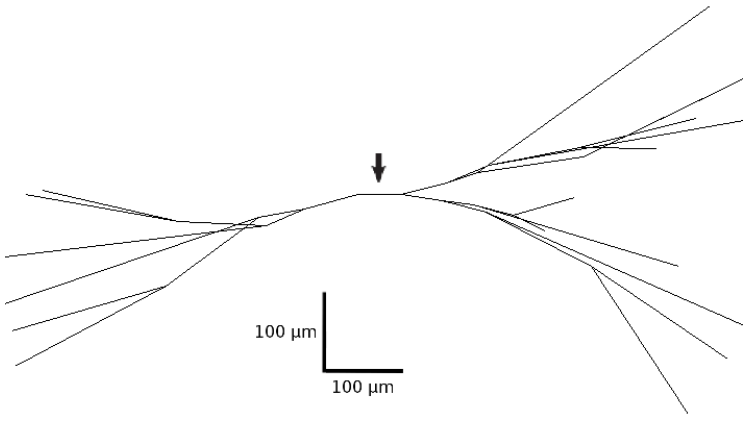

Figure 2.1: ***Illustration of the NEURON representation of the (*Gillies and Willshaw, 2006*) model of a typical rat STN neuron. The arrow indicates the position of the soma, as the diameter of the sections is not shown by NEURON, making the soma difficult to recognize***

The Gillies and Willshaw model does not include the cell's axon, because their study focussed on describing the dynamical behaviour of the typical STN neuron and for that the axon was not considered a significant contributor. As it plays no significant role in the generation of the LFP since the LFP is mainly generated by the relatively large current sources and sinks at the synapses, soma and the dendritic tree **(*Buzsáki, 2012*)**, no axon was added to the model.

Modifications

Two modifications have been made to the Gillies and Willshaw model: While in the original model the membrane of each element of the cell contains a certain distribution of the aforementioned ion channels, these were mostly omitted from the model during this study. Only the soma has kept the active membrane, while all dendritic elements only have passive properties (i.e. a leak current that depends on the RC properties of the membrane) which **(*Gillies and Willshaw, 2006*)** defined to be as described in table 2.1).

Table 2.1: ***Passive membrane properties of the typical STN projection neuron according to (*Gillies and Willshaw, 2006*)***

Passive Property	Value
Membrane time constant	12.8 ms
Capacitance	1.0 μF cm^2
Membrane resistance	12,753 Ω cm^2

The second modification is the insertion of two new sets of membrane mechanisms into the NEURON model ('*extracellular*' and '*xtra*'), which enables NEURON to record extracellular potential fields as a result of current that passes through the cell membrane.

The latter mechanism makes it possible to keep track of all transmembrane currents in order to construct an (extracellular) LFP. In the Gillies and Willshaw model, the different elements in the model cell (i.e. the soma and all dendritic sections) are divided into a number of segments, based upon the overall length of a particular element. In order to determine the LFP that is generated at a certain moment in time and is recorded at a virtual measuring electrode, NEURON goes through a number of steps:

- For a certain segment, the distance between the centre of that segment and the measuring electrode is calculated.
- This distance and the properties of the purely resistive medium are then used to calculate the transfer resistance between the centre of the segment at position *x* and the recording electrode (R_x). This resistance is based on a tissue conductivity of 0.3 Siemens per meter **(*Ranck, 1963; Butson and McIntyre, 2005*)** or 333 Ohm centimetre, and the distance between the centre of the segment and the recording electrode.

- For the next step, all individual currents that pass the membrane of the segment due to leakage and any available ion channels during that specific time step are calculated and combined into the net membrane current (I_m). For this an equivalent electrical circuit of the cell membrane is used, an example of which can be seen in figure 2.2.
- The contribution of that particular segment on the total LFP that is measured at the electrode at that particular time then follows from Ohm's law:
-

$$\boldsymbol{E_{LFP} = R_x \cdot I_m} \qquad \textbf{[1]}$$

with E_{LFP} the contribution of that particular segment on the total LFP in [V], R_x the total resistance between the centre of the segment and the recording electrode in [Ω] and I_m the net membrane current in [A].

By following this algorithm on each time step in the simulation and for each segment in the modelled cells, the entire LFP as recorded by the electrode is constructed.

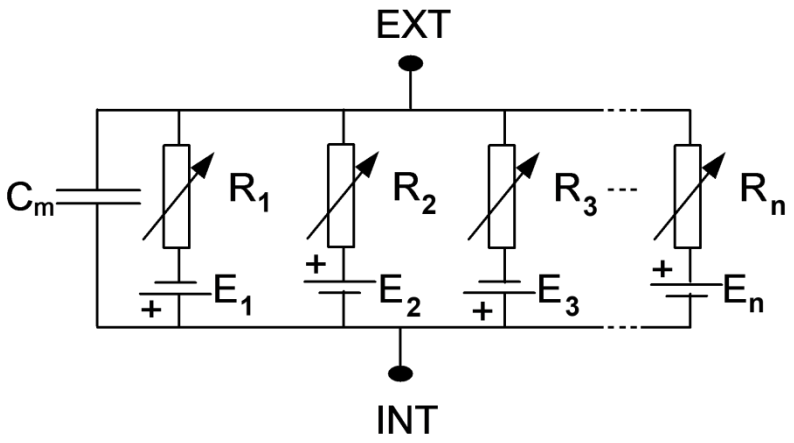

Figure 2.2: ***An example of the equivalent electrical circuit of the cell membrane. Each variable resistance is a model for one type of ion channel and its value depends on the present conductance state of that channel. Each resistance is accompanied by a voltage source, which models the reversal potential for that specific ion type. The capacitor is a model of the membrane capacity. If the internal and external potential (i.e. the potential on both sides of the membrane) and the states of each of the present ion channels are known, the net transmembrane current can be calculated (*** **Malmivuo and Plonsey, 1995*****)***

2.1.2 The Synapse Model

In this study, two types of synaptic projections onto the STN are simulated: excitatory input from the MC and inhibitory input from the GPe. The synapses that are used to simulate these projections are modelled using a virtual synapse that is a part of NEURON, the '*exp2syn*' synapse **(*Carnevale and Hines, 2006*)**. This model generates a post-synaptic membrane current after receiving a trigger signal. Its behaviour is described by the following equations:

$$i_m = G \cdot (v - e) \qquad [2]$$

$$G = weight \cdot (e^{-t/\tau_2} - e^{-t/\tau_1}) \qquad [3]$$

where *weight* is the maximum transmembrane conductance that is induced by the active synapse and therefore determines the maximum amplitude of the resulting membrane current, *v* is the post-synaptic voltage and *e* is the typical reversal potential for the synapse type.

This current is shaped by two time constants, one for the rising flank and one for the decay of the change in neuron membrane conductivity that results from activity of the synapse. By setting these time constants and using *weight* to manipulate the maximum membrane current resulting from synaptic activity, this synapse model is adjusted to approximate the desired type of synapse.

The time constants and peak conductance amplitudes of the different synapse types that are implemented during these simulations are determined based on **(*Destexhe et al, 1998*)**. These parameters are collected in table 2.2 and the transmembrane currents as a function of time resulting from a single synapse of each of the three types are depicted in figure 2.3 along with the transmembrane currents that result from their simulated counterparts.

As can be seen in figure 2.3, the shape and time course of all three synaptically induced currents are similar to those proposed by Destexhe except for the amplitude of the simulated AMPA current, which is at odds with his results: In Destexhe's plot of the current, the peak amplitude is approximately 300 pA according to the scale that was included in the plot, where the simulated synapse only reaches 40 pA. In the text of his paper, however, Destexhe describes the maximum amplitude of the AMPA synapse current to be between 10-30 pA, which shows that the simulated synapse in the current research is indeed conform Destexhe's model and implies a typographical error in the figure.

Motor cortex synapses

The synapses that project from the motor cortex towards the STN are predominantly glutamatergic. This means that they cause excitatory post-synaptic potentials, or EPSPs. As these simulations are based upon experiments that used brain material from rat and the glutamatergic synapses in the rat STN are predominantly a combination of the AMPA- and NMDA-type **(*Clarke and Bolam, 1998*)**, the synapses that are modelled in these simulations will be an even distribution of both synapse types (i.e. 50% AMPA, 50% NMDA).

Globus Pallidus externus synapses

Synapses from afferent projections onto the STN that originate in the GPe are of a GABAergic nature, and are therefore inhibitory (i.e. they cause inhibitory post-synaptic potentials or IPSPs). As GABA receptors in rat are mostly GABA-A **(*Marani et al, 2008, pp. 21*)**, this is the type of GABA synapse that will be modelled.

Table 2.2: ***The time constants and amplitudes of the three synapse models***

	τ_1 in seconds	τ_2 in seconds	Amplitude in nano Siemens
AMPA	$2.73 \cdot 10^{-4}$	$2.3 \cdot 10^{-3}$	0.675
NMDA	$9.1 \cdot 10^{-3}$	$56.8 \cdot 10^{-3}$	0.305
$GABA_A$	$2.73 \cdot 10^{-4}$	$2.3 \cdot 10^{-3}$	0.725

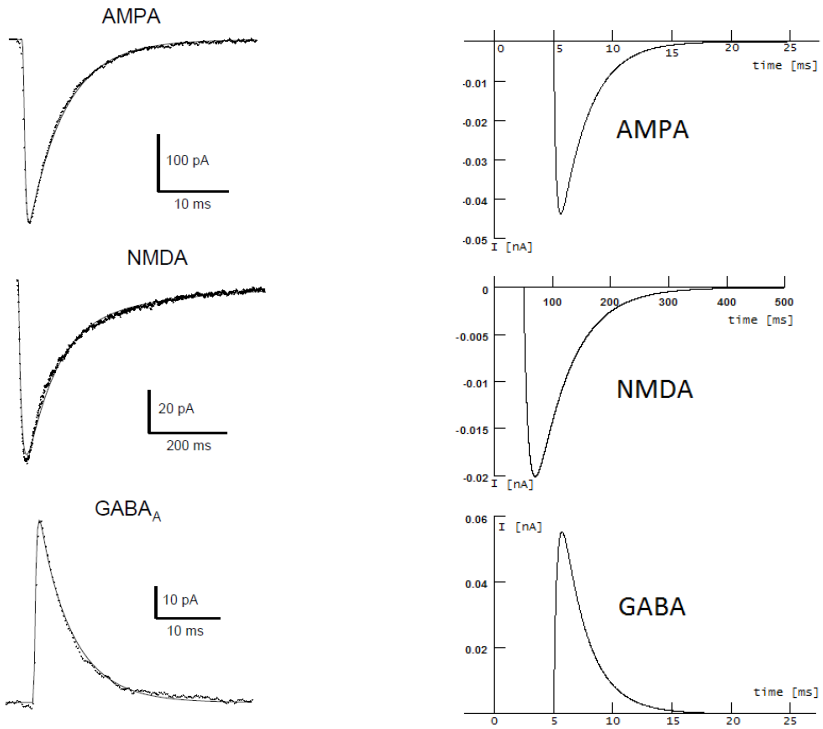

Figure 2.3: ***Left) Transmembrane currents due to single synapse activity as proposed by (*****Destexhe, 1998*****). Right) Transmembrane currents due to single synapse model activity during simulations in this study***

2.1.3 Electrode Array

The electrode array that is simulated during this study is a model of the physical array that was used in the experiments by **(*Van Dijk et al, 2012*)**. That electrode is a one dimensional 16-lead electrode with a contact separation of 100 µm which was shifted by 200 µm between measurements along the anterior-posterior or medial-lateral axis in order to construct a three dimensional electrode array of 16x5x4 contacts (see figure 1.7). During the current research this three dimensional array is constructed by repeating simulations four times with the exact same parameters, while a two dimensional electrode array of 16x5 contacts is repositioned to construct the 16x5x4 array (see figure 2.4).

2.1.4 Synapse Placement

To manage the placement of the simulated synapses in a specific area within the simulation (i.e. the aforementioned synapse cloud), a cylindrical volume in which the synaptic input will be located is defined. The centre of this cylinder is placed at the location of the synapse cloud that is defined for that specific simulation (as is described in paragraph 2.2.4).

The amount of simulated synapses in NEURON is limited. Therefore, a limited number of 30 synapses are randomly distributed over all dendritic elements that lie within this volume at the start of each simulation. The cylinder has a radius of 150 µm and a height of 100 µm. The radius of the cylinder is not of great importance, as long as it is large enough to encapsulate all dendritic elements that reach its height (see figure 2.4). The height of the cylinder is determined in combination with the position of the simulated neurons in such a way that for each cell, independent of the neuron's position, there is always a part of the dendritic tree that will lie within the cylinder that contains the synapses.

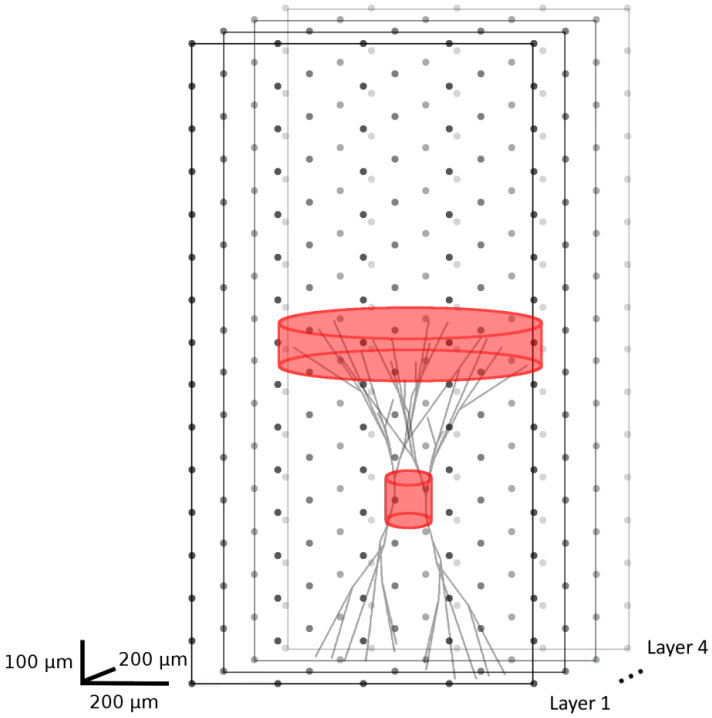

Figure 2.4: ***The 16x5x4 electrode array. In it a cylinder containing the synapses with its centre positioned at (0, 0, 0) and a cylinder containing the somas positioned underneath the synapses holding two neurons at an angle of 0 degrees. The orientation of the neurons is defined as the angle between their longitudinal axis and the vertical axis of the electrode array***

2.1.5 Neuron Placement

To regulate the placement of the simulated neurons, a cylindrical volume is defined in which the somas of all neurons are located. In order to create a balance between keeping the required simulation time in check and using enough individual neurons to create a spatial spread of (return) current sources, 30 neurons will be simulated for each separate experiment. The somas of these neurons are randomly placed throughout the cylinder using a uniform distribution while keeping the longitudinal axis of all neurons parallel to the central axis of the cylinder in which their somas are located. This forms a neuron cluster with a single common orientation. Figure 2.4 illustrates the placement of both the synapse and the soma cylinder.

The location and orientation of the cylinder holding the somas depend on those of the cylinder that contains the synapses, which in turn is a variable throughout the simulations. The soma cylinder is placed coaxial to the synaptic cylinder, with the centres of both cylinders 375 µm apart. Along with a certain height of the soma cylinder, this ensures that dendritic elements from a randomly placed neuron will always reach into the synaptic cylinder.

The dimensions of the cylinder are determined by the restriction that the neuron density within it should mimic the rat STN (i.e. 28750 cells per mm^3) **(*Hardman et al, 2002)*** and the fixed number of neurons (i.e. 30 cells) used during this study. The length of the cylinder is chosen in such a way that each neuron will always have at least a part of its dendritic tree within the cylinder that contains the synapses. Considering the height of the upper dendritic tree above the soma, the length of the cylinder is determined at 100 µm. All requirements then result in a cylinder radius of 57.6 µm.

While the upper dendrites will be (partly) located in the synaptic cloud, the lower dendritic tree is not and will not receive synaptic input. This section of the neuron will therefore only function as conductor, contributing to the generated LFP by sourcing a part of the return current.

2.2 Simulation Variables

Throughout the series of simulations, four different variables are defined which together form a set of parameters for each simulation.

2.2.1 Input type

The input that is supplied to the synapses will simulate the signal resulting from a single stimulus that is given in the motor cortex. As this stimulus travels along the different thalamo-cortical and basal ganglia pathways, it results in a stereotypical multiphasic LFP as described in **(*Magill et al, 2004*)** and is depicted in figure 1.8.

In this study, the different typical peaks of this multiphasic response are simulated individually. This is done by using the appropriate type of synapse that is specific for the peak which is currently simulated and by measuring the LFP response that this configuration produces using a simulated electrode array. That is, peaks N_1 and N_2 are modelled by simulating excitatory projections using an equal mix of (excitatory) AMPA and NMDA synapses, while P_1 and P_2 are simulated using (inhibitory) $GABA_A$ synapses to model inhibitory projections. The cloud of synapses that is used to simulate the projection area is either positioned in the centre of the electrode array or at a position offset from the centre of the array to mimic the results from the *in vivo* experiment of ***(Van Dijk et al, 2012)*** (described in paragraph 2.2.4).

Since there is no actual stimulation of the MC during the simulations and therefore no time reference t_0 is defined yet, the mean timing of the peak at N_1 will be used as main reference for the other elements (listed in table 2.3). The LFPs that result from simulating the individual peaks will later be shifted in time to place them at the correct time intervals with respect to each other and, by means of linear superposition, all four LFPs are then combined into a single LFP (as is explained in figure 2.7 and paragraph 2.4).

Each of the peaks in the stereotypical LFP that was described by Magill is caused by the same stimulus in the MC, which takes a different route through the thalamo-cortical and basal ganglia circuit towards the STN for each one. Each of those routes consists of many different parallel neurons, some of which are slightly faster than others. The stimulus responsible for one of the peaks will therefore reach the STN not as a single spike, but it will be distributed over a certain time interval.

This is modelled by timing the activation of the projection synapses according to a truncated Gaussian distribution. For this distribution the mean value and standard deviations for each of the peaks are respectively based on the time that corresponds to the centre of the peak and the peak widths found by **(*Magill, 2004*)** for each peak (illustrated in figure 1.8 and quantified in table 2.3). The distribution is truncated, meaning that the probability is set at 0 at times that are larger or smaller than the mean plus or minus the standard deviation respectively.

Table 2.3: ***Timing properties of the four characteristic elements that make up the evoked LFP that was recorded by (Magill, 2004). t_0 is defined at the centre (i.e. the mean value) of peak N_1***

	Mean value with respect to t_0 in milliseconds	Standard deviation in milliseconds
N_1	0.0	3.5
P_1	5.9	4.0
N_2	12.1	9
P_2	26.1	7.5

2.2.2 Synaptic Density

Since the number of available synapses is limited (see paragraph 2.1.4), variations in synaptic density are simulated by manipulating the amount of current that is injected by a single synapse. That is, an increase of the number of synapses by a factor two is simulated by doubling the transmembrane current that results of the present synapses, while the number of synapses remains the same. This is done by increasing the *weight* factor in equation [3] (e.g. a doubling of the transmembrane current requires a doubling of this factor).

By applying this method four 'synapse densities' are simulated using 1x, 2x, 3x and 4x the normal transmembrane current in the post-synaptic cell due to activation of a synapse, referred to as a synaptic density of 100%, 200%, 300% and 400% respectively. The normal level of current due to any of the three synapse types is taken from **(*Destexhe et al, 1998*)** and is described in table 2.2.

2.2.3 Orientation

The effects of the orientation of clusters of neurons within the STN are investigated by constructing simulations in which the cylindrical volume that holds the simulated synapses is rotated to a certain orientation with respect to the electrode array. During such a rotation, the centre of the cylinder remains in the location that is dictated by the simulation (i.e. either in the centre of the electrode array or in a position relative to that centre for simulation of the two individual projection areas , as is described in paragraph 2.2.4). The cylindrical volume holding the somas of the neurons for the simulation at hand is defined to be coaxial with the synapse cylinder and to maintain a specified distance between the centres of the two cylinders. Therefore this cylinder will follow the same rotation while its centre is relocated in the electrode array (see figure 2.5).

Four different neuron orientations are simulated: 0°, 45°, 90° and 180° in the coronal plane (i.e. the X-Y plane in figure 2.4) with respect to the vertical axis.

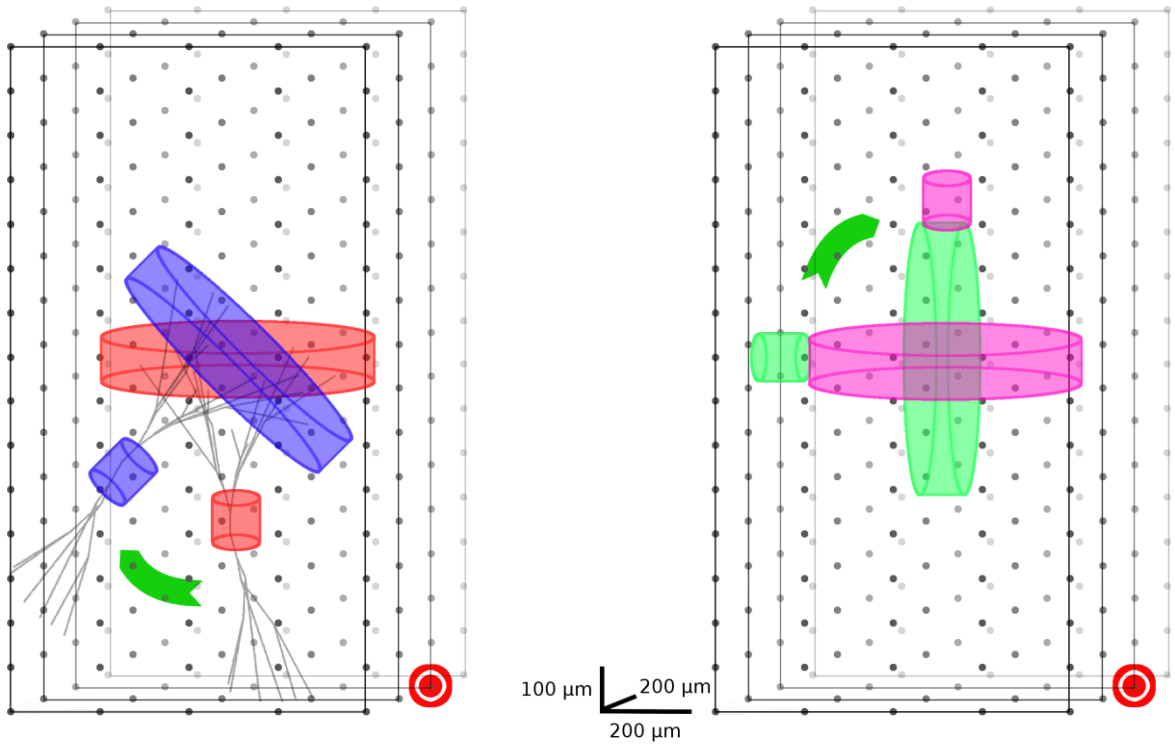

Figure 2.5: ***Illustrations of the electrode array with cylinder combinations for equal source positions on simulated orientations of (left) 0° (red), 45° (blue), or (right) orientations of 90° (green) and 180° (magenta). The arrow indicates the rotation. The recording electrode at position (400, -800, 100) is indicated in red***

2.2.4 Location of the synapse cloud

Two different types of simulations are defined by the position of the synaptic cloud (and therefore also the position of the neurons). In the first, both the synapses that belong to the projections from the motor cortex and the GPe are located in the centre of the electrode array. That is, both types of synaptic input will be at the same position. The second series of simulations places the two different types of synaptic input in individual locations. These locations are chosen in such a way, that the positions of the two synaptic clouds relative to each other are conform the locations of the sources that were found by **(*Van Dijk et al, 2012*)**.

The synaptic clouds are positioned relative to each other in the (coronal) XY-plane, placing both clouds at equal distance from the middle of the electrode array. The centre of the cylinder containing the synaptic input from the motor cortex is placed at (-50, -25, 0) µm, and the centre of the cylinder holding the GPe synapses at (50, 25, 0) µm, as is illustrated in figure 2.6.

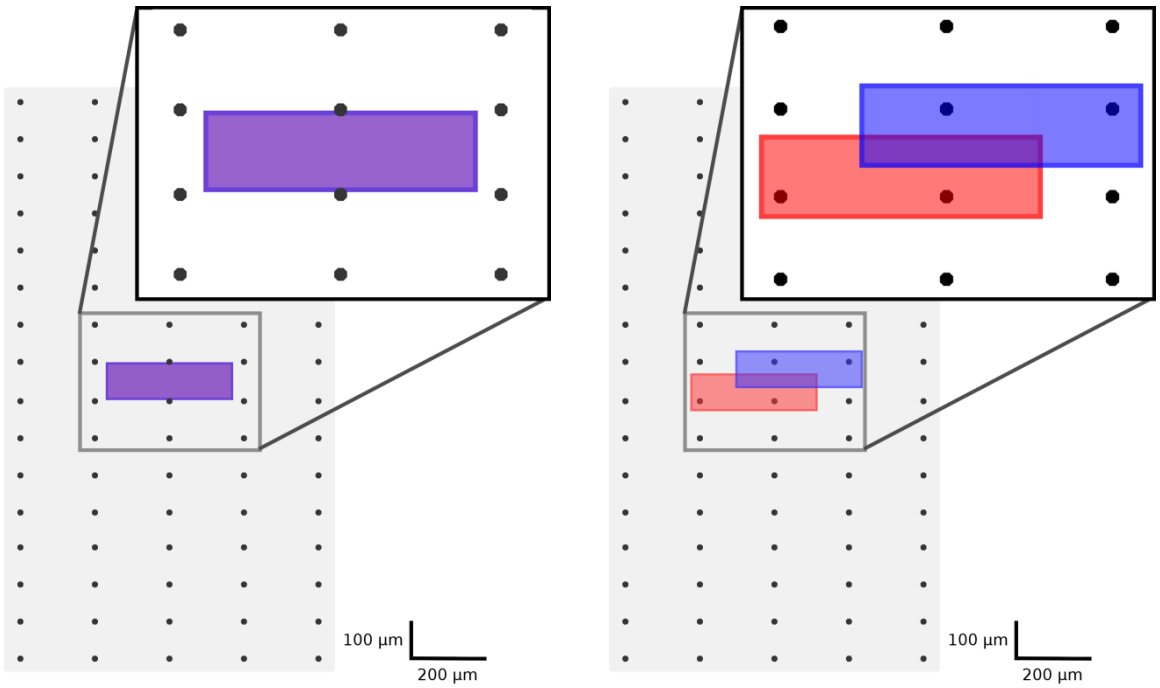

Figure 2.6: ***Two dimensional illustration of the different synaptic locations within the electrode array; (Left) both the excitatory (red) and inhibitory (blue) cylindrical synapse clouds are centred in the middle of the electrode array (the centres of both cylinders are located at coordinates (0, 0, 0)). (Right) The centre of the cylinder containing the excitatory synapses is positioned at (-50, -25, 0) while the centre of the inhibitory synapse cloud is positioned at (50, 25, 0), applying the relative positions of the synapse clouds found by (Van Dijk et al, 2012)***

2.2.5 Simulating the LFPs

From the different variables that are discussed in the previous paragraph unique sets of parameters are compiled. Each of these sets is then used to run a simulation. That is, a simulation is done for each of the orientations, with each of the synaptic densities, for all four types of synaptic input (i.e. the input associated with peaks N_1, P_1, N_2 and P_2) and with these synaptic clouds at either the centre of the electrode array or at their individual locations. This creates 128 unique sets of parameters.

Four simulations are done for each of these unique sets whilst the synapses and neurons are randomly placed in their respective cylindrical volumes for each of those simulations. The recordings resulting from these simulations are then averaged into a single LFP, in order to eliminate the possible influence of the absolute positions of the synapses and neurons.

The time step of these simulations is set at 0.25 milliseconds, resulting in a virtual sampling frequency of 4 KHz. This is over twice the sampling frequency that was used by **(*Van Dijk et al, 2012*)**.

2.3 Data Analysis

The data that is generated during the simulations in NEURON is stored in files, which are then read into MATLAB R2012b (Mathworks, Natick, USA) for further processing and analysis. This analysis consists of two different methods: first both a qualitative and a quantitative analysis of the effects of the different variables on the generated LFP are performed using a single measuring electrode. The second method analyses the spatial distribution of the generated LFP during synaptic activity using the recordings of all 320 electrodes. Both of these analyses are described in this paragraph.

Removing Offset

The recorded LFPs at different electrodes were observed to have individual offsets. These are possibly caused by very slow current leakage which influences the net transmembrane currents in different parts of the simulated cells. In order to avoid problems during the combination of LFPs due to differences in over-all signal levels, these offsets are removed by subtracting the signal level at the first recorded sample from all other samples of that specific LFP for each recorded signal.

Filtering

All recorded LFPs are low-pass filtered using a second-order Butterworth filter with a cut-off frequency of 300 Hz. Any information at higher frequencies than this is not to be considered part of the LFP **(*Buzsáki, 2012*)**.

Combining Peaks

To combine the four different peaks that were simulated into a single evoked LFP as was recorded by **(*Magill, 2004; Van Dijk et al, 2012*)**, the individual peaks are shifted in time to place them at the correct moment in the recording. Please refer to table 2.3 for the amount of time that each peak is shifted. The resulting LFPs are then combined into a single one as is illustrated in figure 2.7.

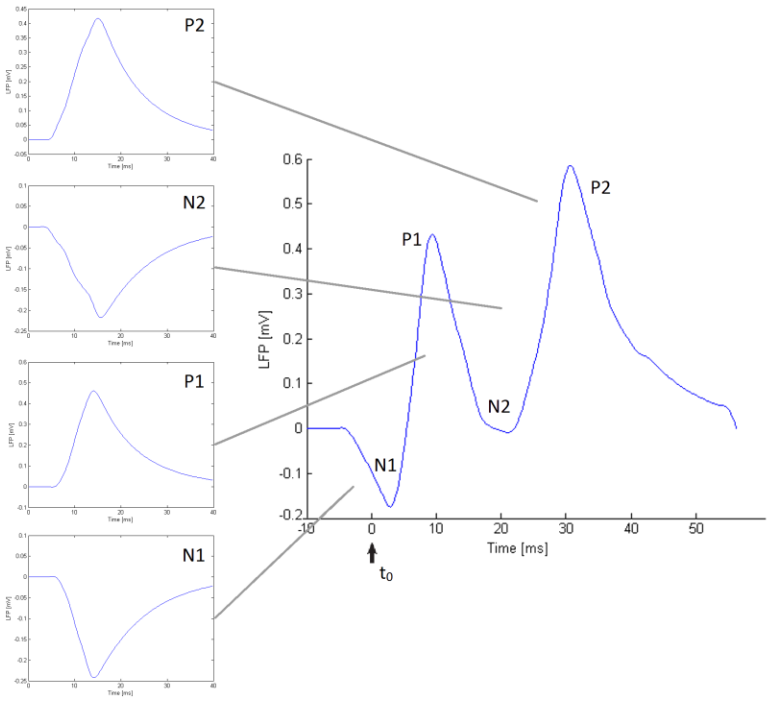

Figure 2.7: ***Combining the four separately simulated peaks into a single typical evoked LFP as proposed by (*****Magill, 2004*****). An arrow indicates t_0 (i.e. the mean value of peak N_1). The LFPs that are shown in this figure are recorded under baseline conditions using the electrode positioned at (0, 200, 100) (i.e. directly above the source of synaptically induced transmembrane current, hence the fact that the polarity of the LFP matches those that were recorded by (*****Magill, 2004*****) and (*****Van Dijk, 2012*****)***

Recording Electrode

To make a comparison between the LFPs that are generated by simulations using different parameter sets, a single electrode in the array is chosen. All signals that are to be compared to others will be recorded on this electrode.

As this study focusses on LFPs, the electrode is chosen to maximize the distance between the electrode and the transmembrane current sources. Also, because the orientation of the simulated neurons varies in a single plane (i.e. the coronal or in this case the XY-plane), the electrode should lie in that same plane to maximize the effect of the variation in orientation. However, due to the dimensions of the electrode array, no electrode lies in the exact plane of the rotation. Therefore the electrode position is chosen in one of the two layers in the electrode array nearest to the plane of rotation. These considerations lead to the electrode which is positioned at [400, -800, 100] µm (indicated in figure 2.5). This electrode is favoured above for instance the electrode at (-400, -800, 100) µm, as the distance between the latter electrode and the simulated neurons will be decreased for simulations for which the neuron orientations are 45° or 90° as can be seen in figure 2.5.

Baseline

A baseline measurement is chosen to which all other measurements are compared quantitatively. This baseline is formed by the evoked LFP that results from an orientation of 0 degrees, a simulated synaptic density of 200% (Appendix I) and with all sources positioned in the centre of the electrode array.

Combined Orientations

In order to investigate the effect of the presence of neuron clusters with a variety of orientations, several of the LFPs that are simulated at single orientations are combined into a number of new LFPs that would be recorded in the presence of those neuron configurations. This is done post-simulation by using linear superposition to combine single orientation LFPs and dividing the resulting signal by the number of LFPs that are involved, in order to maintain the correct signal levels. This way, the following combinations of orientations are constructed: 0° + 45°, 0° + 90°, 0° + 180° and 0° + 90° + 180°.

Contour Plots

To visualize the spatial distribution of the electrical activity in the electrode array, the potential that is registered at all of the individual electrodes in the array is recorded at the time where each of the peaks (i.e. $N_1..P_2$) reach their maximum amplitude. These potentials are then plotted into two dimensional contour plots, one for each of the four layers of the array (these layers are indicated in figure 2.4). Such a set of plots shows how the local potentials that result from the evoked activity vary spatially and which regions produce stronger potentials than others. This distribution of potential indicates the location of transmembrane current sources. By rendering them for each of the combinations of neuron orientations, these plots provide insight into how the LFP throughout the STN is affected by the distribution and orientation of the neurons and their synaptic input. These results are then compared to the CSDs that were reported by **(*Van Dijk et al, 2012*)**.

3. Results

3.1 Variations in Simulated Synaptic Density

Measurements of the LFP on the appointed recording electrode for the different levels of transmembrane current resulting from synaptic activity (i.e. the simulated difference in synaptic density) yield that the amplitude of the LFP is highly dependent on this factor. They also show that the two highest levels cause the peaks that correspond to the inhibitory synaptic activity to reach very high amplitudes relative to those corresponding to the excitatory activity as is plotted in figure 3.1. Also refer to appendix I.

Due to the position of the measurement electrode relative to the current sources in the simulated cells, the polarization of the recorded LFP is opposed to that of the LFPs measured by **(*Magill, 2004*)** and **(*Van Dijk, 2012*)** (see figures 1.8 and 1.9). This effect can be observed in the results presented in paragraph 3.2 and beyond, and is discussed in paragraph 4.1.

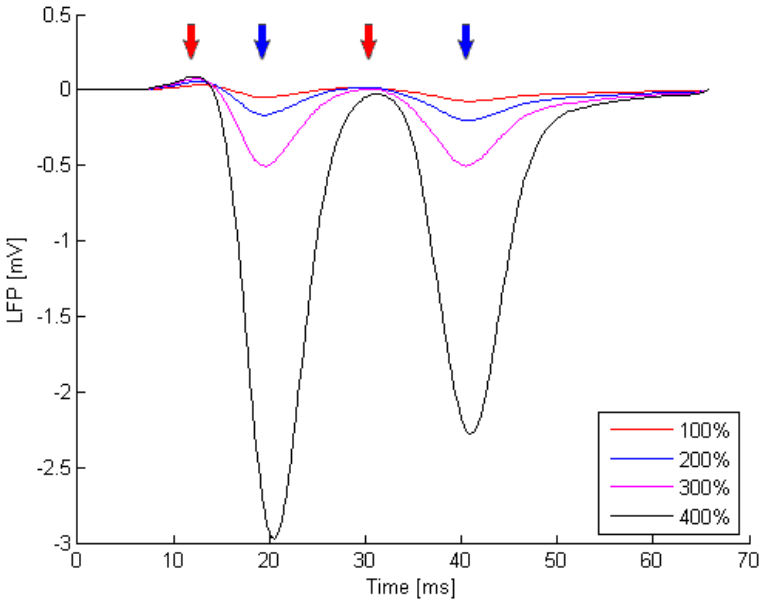

Figure 3.1: ***The LFPs that were recorded using the simulated measurement electrode for all four simulated synaptic densities. Please refer to paragraph 2.2.2 for their definition. The arrows indicate the mean time of the different stimuli, red for excitatory (MC) and blue for inhibitory (GPe) input. Other than the synaptic density, all conditions are conform baseline.***

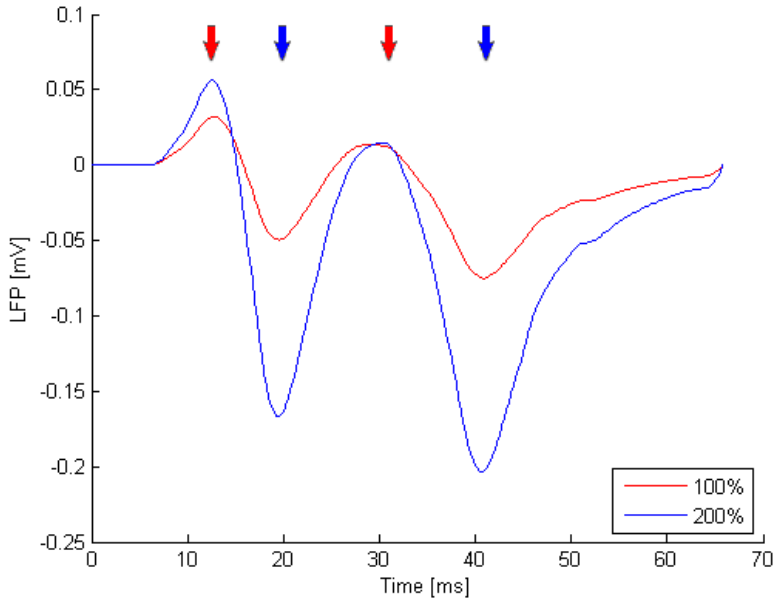

Figure 3.2: ***The LFPs recorded at the measurement electrode for 100% and 200% simulated synaptic densities, showing clear differences in amplitude. The arrows indicate the mean time of the different stimuli, red for excitatory (MC) and blue for inhibitory (GPe) input. Other than synaptic density, all conditions are conform baseline***

The maximum values of the individual peaks in the LFP as a result of the various synaptic densities were measured and expressed in a percentage of the baseline value (marked 'BL: '). Both the amplitudes of the peaks and their percentage of the baseline are presented in table 3.1.

Table 3.1: ***Amplitudes of the individual peaks in combined LFP as a result of variation in the synaptic strength, expressed as both the measured potentials (after normalizing, please refer to paragraph 2.4) and as a percentage of the baseline amplitude***

Recorded Peak Amplitudes

	400%	300%	200%	100%
N1	1,23E-01	0,1005	7,39E-02	4,12E-02
P1	-3,09E+00	-5,97E-01	-2,33E-01	-8,55E-02
N2	0,1117	9,10E-02	6,64E-02	3,68E-02
P2	-2,28E+00	-5,08E-01	-2,07E-01	-7,77E-02

Percentage of Baseline Peak Amplitudes

	400%	300%	200%	100%
N1	166,19%	136,01%	100,00%	55,81%
P1	1328%	256,55%	100,00%	36,73%
N2	168%	136,96%	100,00%	55,37%
P2	1100%	244,89%	100,00%	37,47%

3.2 Variations in Neuron Orientation

The influence of the orientation of a single cluster of neurons on the LFP that is recorded at the measurement electrode is very large, as can be seen in figure 3.3. Depending on the orientation of the neurons, the inhibitory input results in either a positive or negative deflection in the LFP, while the excitatory input has the opposite result. An absolute representation of the LFPs can be seen in the right portion of figure 3.3. Other than the orientation, all parameters for the LFP in this figure follow baseline conditions.

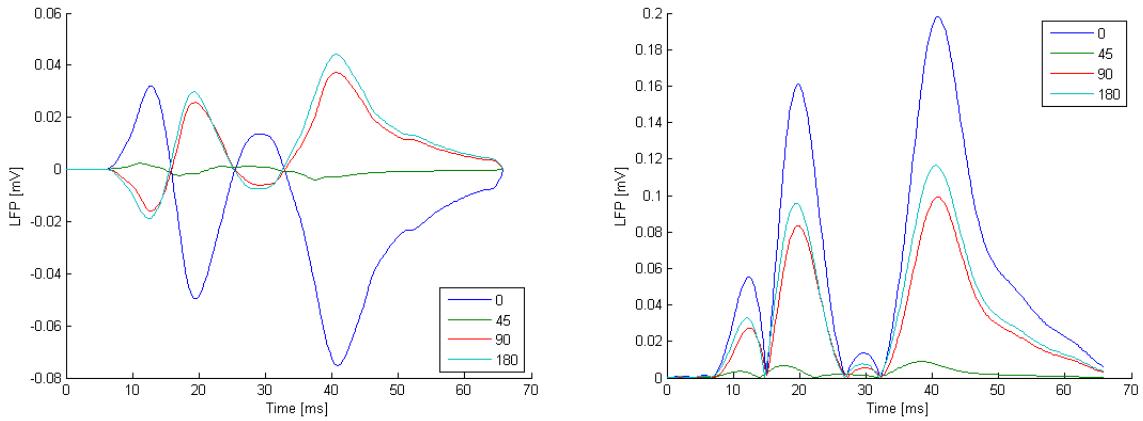

Figure 3.3: ***Left) The LFPs that were recorded using the simulated measurement electrode for neuron clusters at all four individual orientations. Right) A rendering of the absolute levels of the LFPs in which it is clear that a 0 degree rotation results in the largest LFP. Rotations of 90 and 180 degrees return similar LFPs while rotating the neurons 45 degrees yields only a very small LFP. Other than the orientation of the simulated neurons, all conditions are conform baseline (as defined in this chapter)***

3.3 Effects of Combined Orientations

By making the combinations (defined in chapter 2) of LFPs that are the result from neuron clusters with a single orientation to compile several new LFPs, the effects of the presence of several clusters of neurons that lie at different angles with respect to each other can be observed. LFPs resulting from such combinations are plotted in figure 3.4.

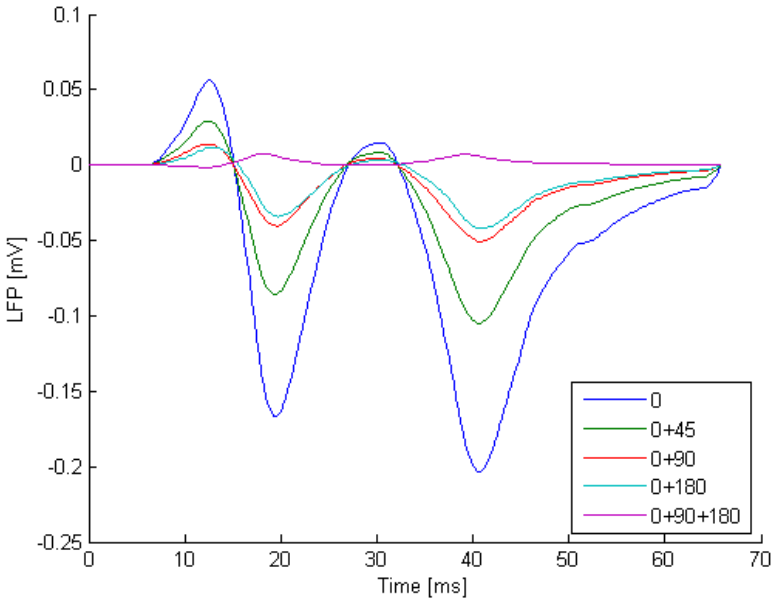

Figure 3.4: ***The LFPs that result from combining the LFPs that were recorded at various orientations. Other than the orientation of the simulated neurons, all conditions are conform baseline (as defined in this chapter)***

In table 3.2 both the recorded voltages and their expression in a percentage of the baseline are given for each peak and each of the orientation combinations. Other than the orientation, all parameters for the LFP in this figure follow baseline conditions.

Table 3.2: ***Amplitudes of the individual peaks in combined LFP as a result of combining the LFPs recorded at various orientations into a single LFP, expressed as both the measured potentials (after normalizing, please refer to paragraph 2.4) and as a percentage of the baseline amplitude***

Recorded Peak Amplitudes

	BL	0° + 45°	0° + 90°	0° + 180°	0° + 90° + 180°
N1	7,39E-02	3,90E-02	1,95E-02	1,56E-02	-1,75E-03
P1	-2,33E-01	-1,21E-01	-5,81E-02	-4,81E-02	8,34E-03
N2	6,64E-02	3,55E-02	1,77E-02	1,41E-02	-1,65E-03
P2	-2,07E-01	-1,08E-01	-5,21E-02	-4,31E-02	7,15E-03

Percentage of Baseline Peak Amplitudes

	BL	0° + 45°	0° + 90°	0° + 180°	0° + 90° + 180°
N1	100%	52,74%	26,39%	21,07%	-2,36%
P1	100%	51,78%	24,98%	20,66%	-3,58%
N2	100%	53,45%	26,64%	21,19%	-2,49%
P2	100%	51,96%	25,17%	20,79%	-3,45%

Plotting the potential that is registered at all of the individual electrodes at the time at which one of the peaks (i.e. $N_1..P_2$) reaches its maximum amplitude results in a set of four contour plots, one for each layer of the array. Doing so for each of the orientation combinations results in a set of plots as seen in figure 3.5. These plots show the situation in which both synaptic projections (i.e. from the MC and the GPe) are at the same location. The plots that result from these projections having an individual location can be found in appendix II.

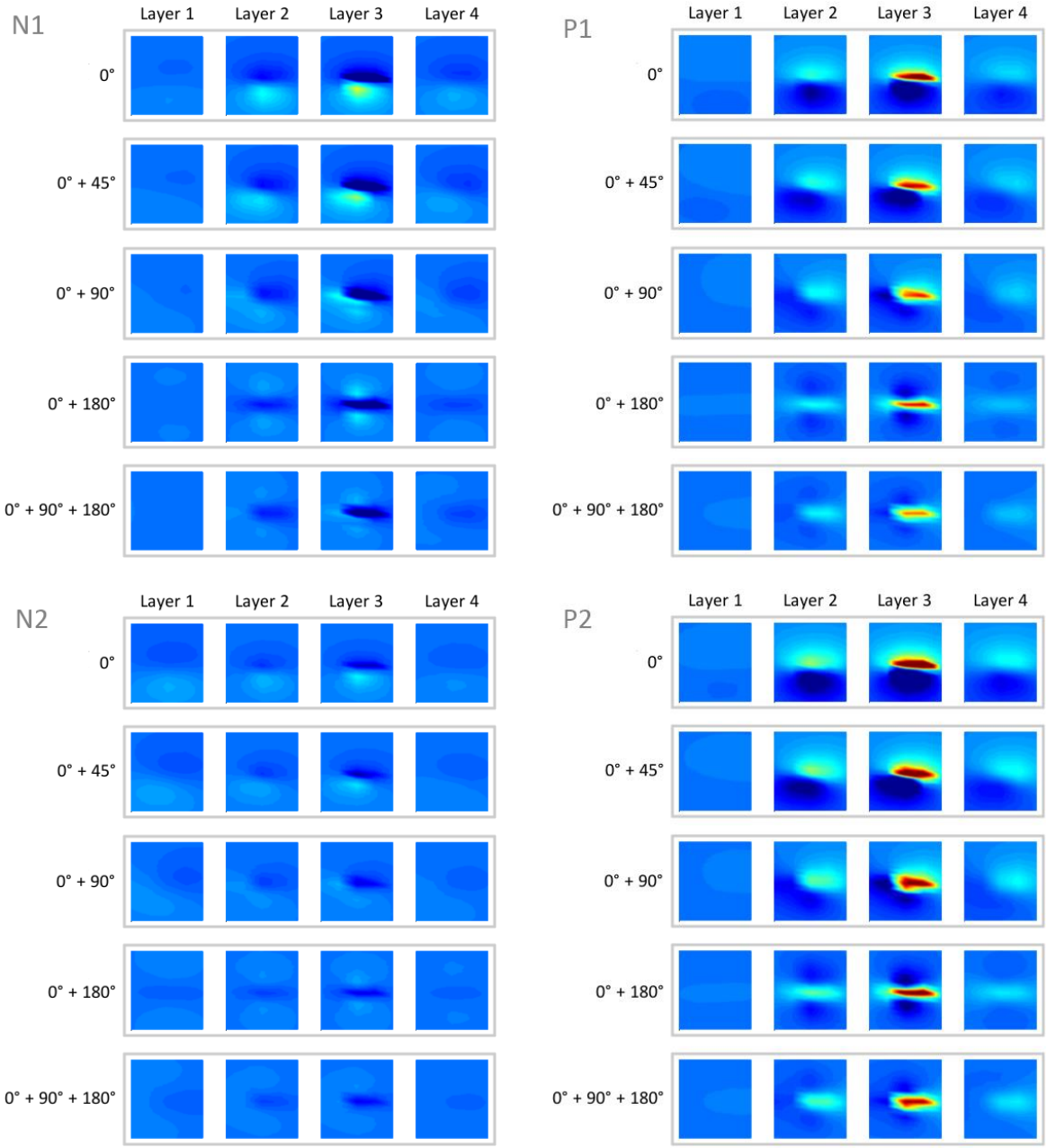

Figure 3.5: ***Four sets of four contour plots (one for each peak) for each combination of neuron orientations as defined in paragraph 2.2.3. The layers are as defined in figure 2.4. These plots show the potential that is measured at all individual electrodes at the time of maximum amplitude of peaks N_1, P_1, N_2 and P_2. As the input that causes peaks N_1 and N_2 is excitatory, the transmembrane current at the synapses is directed into the cell. This causes a locally lowered potential at the synapses, while the return current is directed outwardly and shows in these plots as a locally elevated potential. For the inhibitory input that causes peaks P_1 and P_2 the currents flow in the opposite direction and result in inverted potentials relative to the excitatory situation. Other than the orientation of the simulated neurons, all conditions are conform baseline (as defined in this chapter)***

4. Discussion

4.1 Analysis of Results

4.1.1 Simulated Synaptic Density

The fact that amplitude of the peaks in the LFP that are the result of the inhibitory synaptic activity (i.e. P_1 and P_2) increases more for higher synaptic densities is clearly visible in figures 3.1 and 3.2. The cause of this discrepancy between the effects of increased inhibitory and excitatory activity is most likely the difference in the type of synapses that are used for both types of input. While the inhibitory signal is conducted by a single type of synapse, $GABA_A$, the excitatory signal uses two different types, AMPA and NMDA. As can be seen in figure 2.3 and table 2.2, the membrane conductance and therefore the transmembrane current that is induced by the $GABA_A$ synapse is the highest of the three synapse types. While the current that results from an active AMPA synapse is almost of the same magnitude, the maximum current due to an NMDA synapse is much lower than that of its $GABA_A$ counterpart. As half of the excitatory synapses are of the NMDA type, this will result in amplitudes that are lower relative to the $GABA_A$ induced peaks.

To compare: Two active $GABA_A$ synapses result in a change in membrane conductivity of 1.45 nano Siemens, while the combination of one AMPA and one NMDA synapse cause a change of 0.98 nano Siemens. That is, the average change in transmembrane conductivity due to activation of both synapse types during an excitatory input is 67% of that in case of the activation of two $GABA_A$ synapses during an inhibitory input.

As can be seen in table 2.2 the decrease in amplitude when moving from 200% to 100% synaptic density is equal for both excitatory peaks (55%) and for both inhibitory peaks (37%). When this is converted to percentages of growth in amplitude when moving from 100% to 200% synaptic density, it is found that the amplitude of the excitatory peaks increases with 180%, while the inhibitory peaks increase with a much larger 270%. From this it follows that the increase of the excitatory peak amplitude is 67% of the increase of the inhibitory peaks. As this ratio is the same as that was found for the difference in synaptic conductivity, it is concluded that the difference in synaptic conductivity for excitatory and inhibitory synapses is indeed the cause of the uneven scaling of the peaks for an increased synapse density observed during this study.

4.1.2 Neuron Orientation

When analysing the LFPs that are recorded by the measuring electrode (i.e. the electrode positioned at [400, -800, 100] μm) it is clear to see that the orientation of the neurons that generate the LFP is of great influence to the recorded signal (see figure 3.3). By considering the first peak in the LFP (i.e. the excitatory peak N_1) for all four orientations, this influence can be observed.

For an orientation of 0° the recorded N_1 peak is positive while the opposite orientation (i.e. 180°) results in a negative peak. This is because at an orientation of 0° the current source that is nearest to the measuring electrode (i.e. the dominant source) is that of the return currents at the somas. This also account for the fact that, even though the synaptic input is excitatory and one would therefore expect to see a negative deflection in the LFP, the potential at the measuring electrode increases. At an orientation of 180° on the other hand, the dominant source is the synaptic cloud.

The fact that these two peaks have dissimilar absolute amplitudes (see figure 3.3), is due to the distance between the measuring electrode and the two sources. That is, for an orientation of 0° the dominant source (i.e. the somas) are located much closer to the measuring electrode compared to the dominant source (i.e. the synapses) in case of an orientation of 180°, as can be seen in figure 2.5. This causes the dominant source to induce a lower potential at the electrode in the latter case.

While a similar situation causes the polarisation and amplitude of the LFP for an orientation of 90°, the LFP that is generated by neurons that are rotated at a 45° angle is barely measured on the electrode. This is caused by the fact that both sources (i.e. the synaptic input and the return current that is generated mainly at the somas) are at similar distances from the recording electrode. Since both signals are of opposite polarization, they cancel each other out. A close observation of the signal indicates that the small amount of signal that is still recorded has the same polarization as the LFP that was recorded at an orientation of 0°. This is as expected, since at this orientation the centre of the cylinder containing the somas is slightly closer to the electrode (859 µm) than the cylinder holding the synapses (900 µm), causing the effects of the return current (outward for an excitatory input) to be dominant in the LFP.

4.1.3 Combined Orientations

Single Recording Electrode

The effects of combining LFPs of various simulations with single orientations into new LFPs that would result from the presence of multiple neuron clusters at those orientations are shown in figure 3.4 and table 3.2. It is clearly visible that by placing neurons at an orientation other than 0°, the amplitude of the LFP that is recorded by the measuring electrode is decreased. This is as expected.

The fact that the combination of the 0° and 180° neurons does not result in a complete cancelation of signals is due to the fact that the distance between the measurement electrode and the different sources of the LFP is not large enough. That is, while the cylinders that contain the opposing synaptic activity are in the same position and will therefore generally cancel each other out, the cylinders that hold the somas for the neurons of both orientations do not share their location and therefore create two current sources at unequal distances from the measuring electrode. This causes the closest of those sources to remain dominant in the measured LFP.

In the case that is illustrated in figure 3.4, the LFP that originated from the neurons at 0° dominates the measured potential. This is also the case for the combined LFPs of neurons with an orientation of 0° combined with cells at either 45° or 90°. The LFP that results from the combination of 0°, 90° and 180° rotated neurons on the other hand is nearly non-existent. Here the combination of the neurons at 90° and 180° results in an LFP component that is equal and opposing to that generated by the neurons at 0°. At a greater distance from the neuronal structures, it is expected that only the

contribution of the neurons at an orientation of 90° will be measurable due to mutual cancelation of the LFPs of the neuron clusters at the other two orientations.

Contour Plots

Plotting the potentials that are recorded at each individual electrode at a specific moment in time as is done in figure 3.5 shows a clear difference between the situations in which all neurons share the same orientations and where the neurons are divided into clusters that have different orientations.

For instance, while looking at the plots of layer 3 for peak P_1 in figure 3.5, the spatial distribution of the recorded potentials clearly differs between the situations with only the single 0° orientation and with the combination of 0°, 90° and 180°. In both cases the locations of the return current sources are visible, but while in the former case this source is in a single position, in the latter this source is divided over three locations. As for both situations the total amount of return current is the same, the combination of neurons at multiple orientations yields a less focussed source for this return current. This leads to the hypothesis that when potential measurements in the STN only clearly show the effects of a dominant mono-polar source (i.e. a dominant sink or a source, possibly accompanied by opposing sources with lower amplitudes as was found by **(*Van Dijk et al, 2012*)**) at a certain moment in time, the activity that causes this source is highly concentrated relative to the opposing sources (e.g. the return current due to a synaptic input current) which is more spatially distributed. This situation is illustrated in figure 4.1. This indicates that the portions of the neurons that are affected by the synaptic input (i.e. (parts of) their dendritic tree) are all positioned in the area that receives the projections (e.g. from the MC or the GPe) while the orientation of the longitudinal axes of these neurons can be highly diverse for all neurons involved.

The fact that the LFPs that were recorded by **(*Magill, 2004*)** and **(*Van Dijk et al, 2012*)** had the same polarity regardless of electrode depth within the STN would seem to indicate that this scenario is in fact the case. That is, the sources that are created by the synaptic projections coming from the MC and the GPe are highly local, while the somas and the dendritic elements through which the return current flows are spatially distributed throughout the STN. Along with the dimensions of the typical neurons within the STN and those of the nucleus itself, this would make the source due to the synaptic activity dominant over the return current source, regardless of the electrode position within the STN.

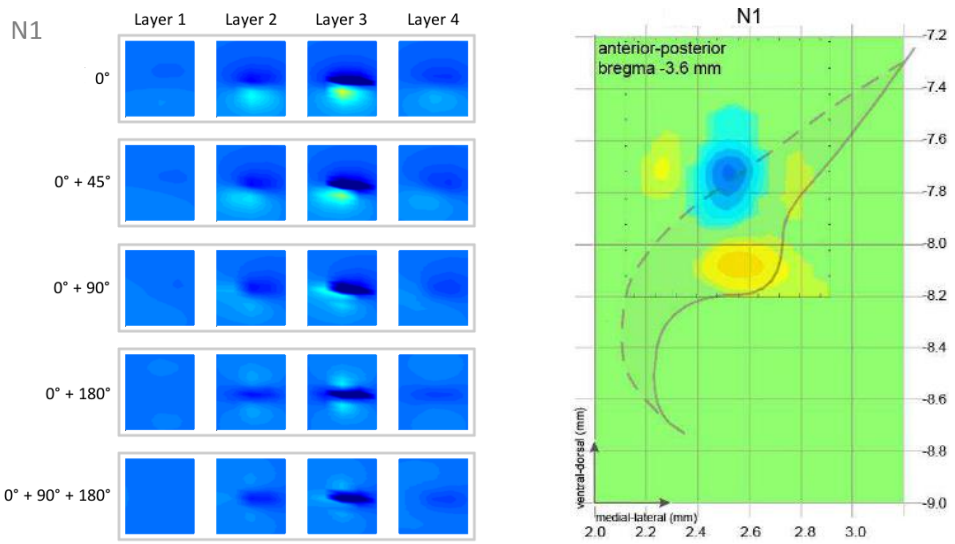

Figure 4.1: Left) The spatial distribution of sources throughout the electrode array for the simulated excitatory input at the time of peak N1. Right) The CSD that was recorded by (*Van Dijk et al, 2012*) for the same peak. In this CSD there is a clear current sink, which is surrounded by three current sources with a lower amplitude. This situation is very similar to the spatial distribution of recorded potentials in layer 3 of the left figure, when simulating a combination of three neuron clusters at different orientations

4.2 Model Validation

In order to validate the model that is used in this study, several aspects and components of it are compared to their counterparts in other studies.

4.2.1 Measuring LFPs?

When the LFP that is measured over a single vertical array of simulated electrodes is compared to the results of a similar simulation done by **(*Pettersen et al, 2008*)**, it is clear that the simulated LFP is qualitatively comparable to the results from Pettersen *et al,* as can be seen in figure 4.2. The apparent differences in amplitude and the reach of the LFP (i.e. Pettersen's LFP shows a strong deflection on more electrodes than the result from the current simulations does) are caused by several factors. Pettersen *et al* simulated over 1000 cells whereas the LFP of the current study is the result of only 30 neurons. Also, Pettersen *et al* used a completely different type of cell (i.e. a cortical layer 5 pyramidal neuron) which has a different morphology than the Gillies and Willshaw STN neuron.

From the qualitative similarities between the current results and those of Pettersen *et al*, it is concluded that the model that is proposed in this research does indeed produce virtual LFPs.

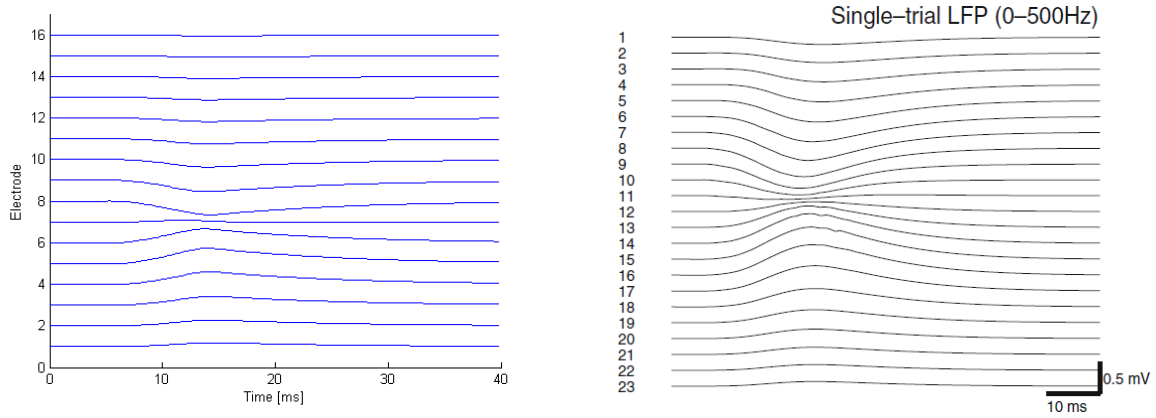

Figure 4.2: ***Left) Simulated LFP on a vertical 16-electrode array for an excitatory synaptic input in Gillies and Willshaw model STN neurons. Right) LFP as was simulated by (*****Pettersen et al, 2008*****) on a vertical 23-electrode array for an excitatory synaptic input in modelled cortical layer 5 pyramidal cells***

4.2.2 Stereotypical Evoked LFP?

Comparing the LFP that results from combining all individual peaks (i.e. N_1, P_1, N_2 and P_2) with the LFP that **(*Magill et al, 2004*)** proposed to be stereotypical for measurements in the LFP after stimulation of the motor cortex, it is clear that both LFPs are qualitatively quite similar. To make this comparison, the simulated LFP was measured at an electrode that was placed above both current sources in the model using a neuron cluster with an orientation of 0° in order to obtain the same signal polarity as was found by Magill.

An obvious discrepancy between the results from **(*Magill et al, 2004*)** and those of the simulations in this study that can be seen in figure 4.3 is the fact that in the *in vivo* measurements the peak of N_2 remains at a slightly elevated potential, while for the simulated LFP N_2 almost reaches the zero potential. A possible explanation would be that (*in vivo*) the peak at N_2 is the result of less synaptic activity compared to the peak at N_1 and would therefore have a weaker influence on the generated LFP. This theory could be tested by decreasing the amount of active synapses while simulating the excitatory input that causes the peak at N_2.

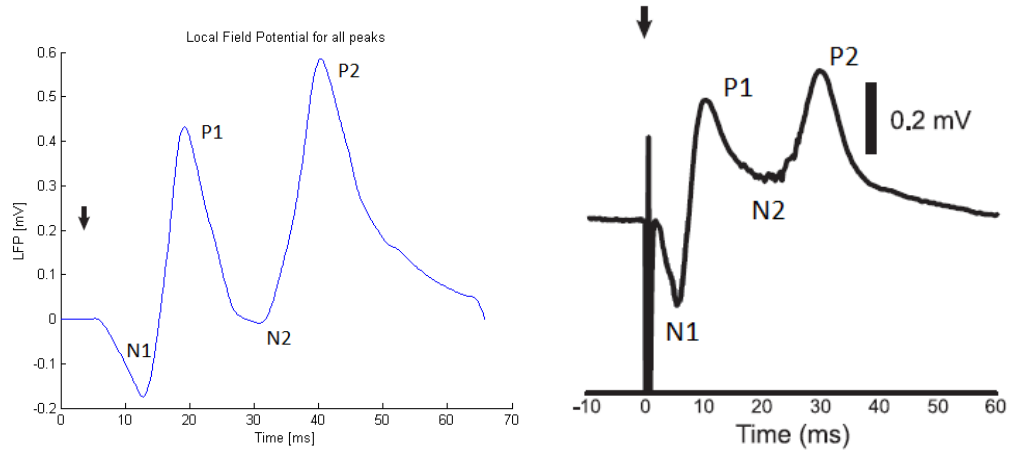

Figure 4.3: ***Left) The resulting signal from simulations of an evoked LFP using the model during the current research and a neuron cluster with an orientation of 0°, recorded by the electrode at (0, 1100, 100) above both current sources. Right) Evoked LFP as recorded* in vivo *in the rat STN by (*Magill, 2004*). The arrows indicate the moment of stimulation in the* in vivo *experiment and the simulated moment of stimulation in the current study***

4.3 Clinical and Research Implications

Nowadays, deep brain stimulation of the STN is the main treatment for PD patients for whom their medication has reached the end of its effectiveness. Although it has therefore become almost a routine procedure, implanting the stimulation electrode at exactly the correct position still proves to be a problem. Since the motor related subsection of the STN is a small target and a slight error in the position of the stimulating electrode can lead to rather severe and unwanted side effects, accurate implantation of the electrode is paramount **(*Hamani, 2004*; *Temel et al, 2006*)**.

One of the main causes of these difficulties lies in the fact that the position of the target nucleus varies between patients, while the equipment that is currently used during the procedure makes accurate imaging through MRI impossible. In order for the electrode to still reach the required position, the suspected target area and its surroundings are probed for oscillatory behaviour that is characteristic for the pathological STN by inserting multiple electrodes for MERs **(*Chen et al, 2005; Rezai et al, 2006*; *Bevan et al, 2002; Brown, 2003; Hammond, 2007; Brown, 2007*)**.

However, the insertion of an electrode in the brain introduces a risk of haemorrhage. It is therefore preferred to use as little probing electrodes as possible before implanting the stimulation electrode and using only a single electrode for both targeting and stimulation is considered ideal. Such an approach would, after implantation in the approximated target area, use directional measurements of LFPs to determine the direction and possibly the distance to the real target area. Once the correct target has been located, directional stimulation through current steering would ensure the optimal stimulation of the target whilst minimising the risk of complications due to haemorrhage **(*Martens et al, 2010*)**.

This approach requires the ability to identify and locate the target area through analysing the LFPs that are recorded by the electrode's many contacts. It therefore requires knowledge about the nature and the extent of the influence that neuronal organization within the STN has on these LFPs. This study has shown the effects of several different factors that can be found in neuronal organizations on the LFPs that are generated by those neurons, and provides a tool for further computational modelling studies in this field.

Using the implanted electrode for both stimulation and measuring of the state of the STN through analysing the directionally measured LFP, a new line of stimulators can be designed that are no longer dependent on medical personnel to set the correct stimulation parameters. These new stimulators can have an integrated computer that analyses the measured LFP and determines the necessary stimulation parameters based on that analysis, therefore creating a closed loop feedback system that reliefs both patient and medical professionals. This would increase patient comfort while saving precious time and money.

4.4 Model shortcomings

4.4.1 Rat versus Human

As there is much more information on the STN of the rat than there is of the human STN due to the amount of *in vivo* research that has been performed on the former compared to the latter, most of the data and models that were used during this research are based on the rat. Mainly, the neuron model that was used during these simulations (i.e. the **(*Gillies and Willshaw, 2006*)** model) is based on cells found in the rat STN. Potentially, a difference in presence and distribution of ion channels between the nuclei in both species could influence the results. Although there are a lot of similarities between the two STNs there are also several differences **(*Hardman et al, 2002*)**, which may reduce the model's accuracy for the human STN.

4.4.2 Passive Dendrites

The Gillies and Willshaw model of the STN neuron was stripped of all its active ion channels, save those in the soma. As the original neuron proposed by Gillies and Willshaw (i.e. with active ion channels in all sections of the model) produced an action potential even for a very small synaptic input, this was done to enable the evocation of subthreshold activity. This approach was also taken by **(*Pettersen et al, 2008*)** while performing similar simulations using cortical cells. Although the resulting LFPs from the adapted model are qualitatively similar to *in vivo* measurements, these adaptions deviate from the model that was designed by **(*Gillies and Willshaw,* 2006)** to mimic the characteristic behaviour of the typical STN neuron. Therefore, these adaptations of the model that was used in the simulations of this study make it less accurately resemble the neurons that are found in the STN.

4.4.3 Intracellular Medium

The simulations in this study are placing the modelled neurons in a virtual intracellular medium that is homogeneous and purely resistive, where the real environment in an STN is nothing of the sort. This is an assumption that allows for the modelling necessary to answer this project's research question, but should be reconsidered if the model that was developed for this study is to be used for further research into the STN.

4.4.4 Synaptic Density

Due to an unresolved programming difficulty in NEURON, it proved impossible to create more than a total of 37 synapses in a single simulation. Because of that and since no absolute information about the realistic synaptic density within the rat STN was found in literature, it was decided that an equal number of synapses and neurons (i.e. 30) would be used and to simulate the presence of a larger number of synapses. The latter is done by manipulating the current that results from a single activated synapse. That is, by doubling this current the presence of two synapses on a particular location on a dendrite is simulated while using only a single synapse.

Using this approach, four different synapse densities were modelled, simulating a total number of 30, 60, 90 and a 120 synapses (i.e. normal postsynaptic transmembrane currents were multiplied with factors 1, 2, 3 and 4 respectively). Due to effects from the use of different types of synapses (described in paragraphs 3.1 and 4.1), the LFPs that resulted from the latter two simulated synapse densities deviate too much from the *in vivo* LFPs found by **(*Magill, 2004; Van Dijk et al, 2012*)** and are therefore considered unrealistic.

4.4.5 Neuronal Density

The current simulations involve a rather small number of neurons. Similar research on LFPs in the cortex by **(*Pettersen, 2008*)** used 1040 cells, while the current simulations use only 30. This choice was made considering the time involved in running the simulations on the available hardware. The current model is suitable for simulations on an increased scale, if either more time or more computing power is available.

4.4.6 Orientations

Presently, the orientation of the simulated neurons is varied in a single plane (in this study the coronal plane). This is done to limit the number of variables and with that the amount of data that is generated during this research. Using the results from this set of orientations, it is possible to answer the research question that is the basis of this study and it also gives insight into the expected results of possible future simulations that involve variable orientations in other planes as well as increasing the number of orientations.

5. Conclusions and Recommendations

In this study the effects of both different orientations and levels of synaptic input on the LFP that is recorded in the STN are explored by means of computational modelling and simulation. The NEURON simulation environment proved to be a powerful and versatile tool for these simulations, as it enables the use of detailed models of the neurons that are characteristic for the STN.

The effects of both the amount of synaptic input and the orientation of the receiving neurons proved to be of influence on the LFP that is recorded in the STN. This was illustrated by analysing the effects on the LFP that is measured at a single location while varying these parameters as well as the effects of the neuron orientations on the spatial distribution of the generated potentials throughout the simulated electrode array. Through inspection of the latter it is suspected that the highly focussed synaptic input in the STN on the one hand and the distributed nature of the opposing return current on the other are indicatory for an absence of organization between STN neurons. That is, it seems that neurons within the STN do not adhere to a (partial) parallel organization as can be found in the cortex. Although results from this study therefore suggest that the longitudinal axes of synaptically activated neurons in the STN may not have a clear organization, their dendritic trees seem to be centralized in the projection areas (i.e. the positions where projections from the MC and the GPe affect the STN). This would suggest that while the dendritic trees of neurons that are connected to a certain projection area are all positioned in that area, these neurons' axes may radiate away from that projection area. This would create a very dense area of synaptic activity whilst distributing the return current sources over a vast region around this area. The current model can be used to perform simulations to investigate this in future research.

The model that was created resulted in simulated LFPs that show a high similarity to *in vivo* measurements which indicates that this model could be used for further research into the STN. As the inner workings of the STN and the mechanisms behind the effectiveness of DBS in this nucleus as a treatment for PD are yet to be fully understood, such further research is essential. Providing a tool for this research is therefore a step towards more knowledge about the disease, better medical procedures to treat it and with that can lead to improved lives for patients that suffer from PD.

Recommendations

For future work in this area, this study indicated several points of improvement and other recommendations:

- The approach in this study has been to simulate the behaviour of a limited number of cells using the simulation environment offered by NEURON. If the simulation of more neurons required, it would be preferable to use NEURON to simulate a single cell under the required conditions and make precise recordings of all membrane currents for each section of the cell. This data can then be used to calculate the external potential as a result of that specific cell at any arbitrarily chosen location relative to it. Through linear superposition of the single cell

recordings, any number of cells can be placed in every required position. This makes for a much more scalable simulation and is less vulnerable to possible shortcomings in the NEURON simulation environment due to scaling. This does however require a different approach for the delivery of the synaptic input. In the current simulations, the positions of the synapses were randomly chosen between sets of four simulations and the resulting LFPs of which were then averaged to decrease the possible influence of the absolute positions of the synapses. An alternative would be the approach that was taken by **(*Holt and Koch, 1999; Pettersen et al, 2008*)**, where synaptic input was simulated by directly manipulating the transmembrane conductivity over a large section of the dendritic tree of a neuron.

- The simulated neurons in this research were given only passive electric properties throughout the cell, except for the soma. In the latter the ion channels that are characteristic for the STN were maintained **(*Gillies and Willshaw, 2006*)**. While this method enabled the model to produce good results, this meant that the entire response to synaptic input is free of action potentials. Similar research such as that of **(*Pettersen et al, 2008*)** included a relatively small set of cells that received suprathreshold input which therefore generated action potentials, while input for the majority of the neurons remained subthreshold. This may have a significant effect on the generated LFP which is not present in the simulations of the current study and would make the model more realistic. Future work should therefore include active cells to assess the effect thereof.

- This study limited the variation of the neuron orientation relative to the electrode array to a single plane. For future research it is recommended to consider involving rotation in the other two planes as well, in order to reach a higher level of model realism. Also, increasing the number of orientations that are simulated in every plane would contribute to this. Especially distributing all present neurons around the synaptic cloud in order to form a spheroid would make for an interesting simulation.

Appendix I: Redefining Baseline

The over-all shape of the LFP that results from simulated the synaptic densities of 300% and 400% is quite aberrant from the one that is expected based on **(*Magill, 2004*)**. That is, while the latter shows a relatively equal amplitude for both the peaks that result from excitatory input and those that result from inhibitory input, the amplitudes of the inhibitory peaks (P_1, P_2) in the former are very high relative to the excitatory peaks (N_1, N_2), as can be seen in figure A.I.1.

The LFP that results from the simulated synaptic densities of 300% and 400% is therefore considered unrealistic. A new baseline was defined using the 200% synaptic density, as proportions of the amplitudes remain relatively similar to those found *in vivo*, plotted in figure A.I.2.

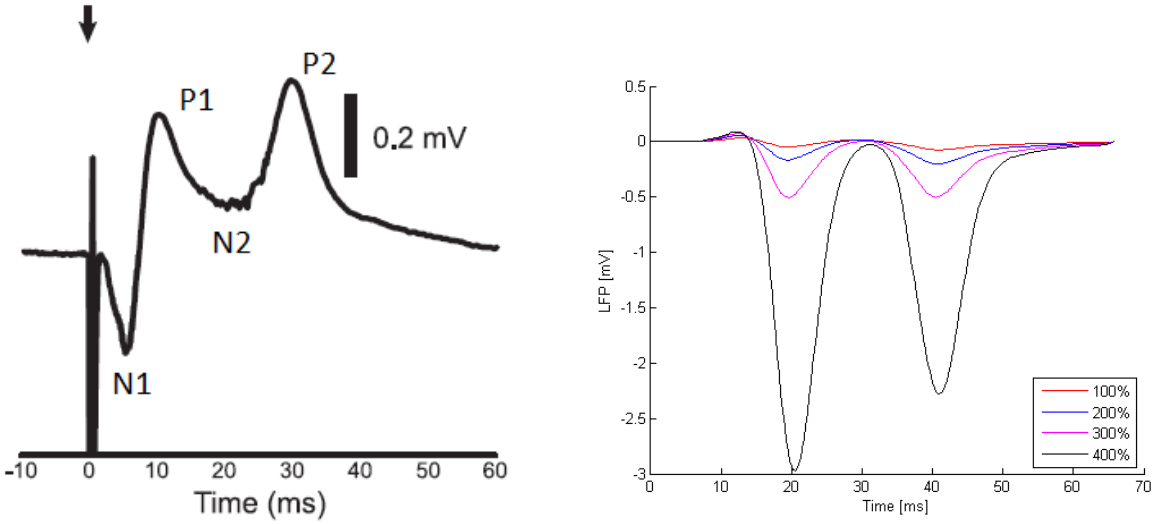

Figure A.I.1: Left: (Reprint of figure 1.8) ***The LFP as was recorded by Magill in the rat STN, following a stimulus in the ipsilateral motor cortex, showing the four characteristic elements in such an LFP. The moment of stimulation is indicated by the arrow. (Figure modified from (*Magill et al, 2004*)).*** **Right: (Reprint of figure 3.1)** ***The LFPs that were recorded using the simulated measurement electrode for all four simulated synaptic densities. Please refer to paragraph 2.2.2 for the definition.Other than the synaptic density, all conditions are conform baseline.***

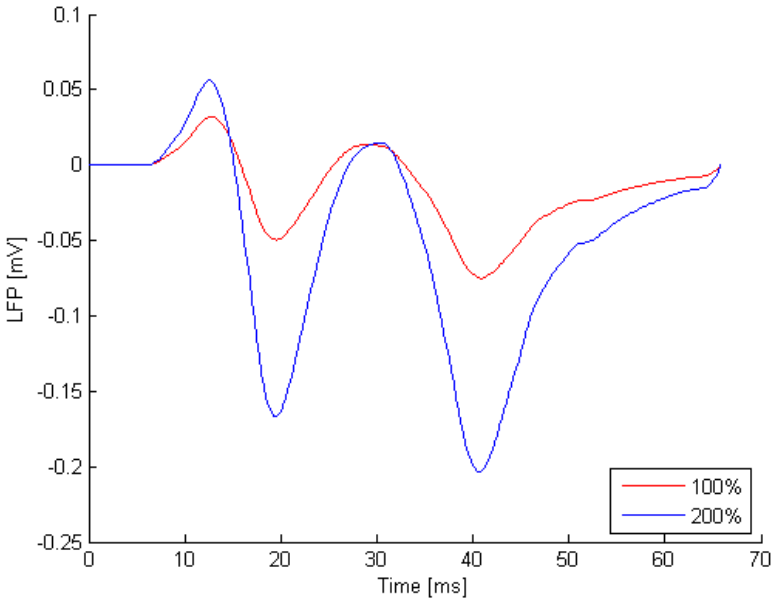

Figure A.I.2 (Reprint of figure 3.2): ***The LFPs recorded at the measurement electrode for 100% and 200% simulated synaptic densities, showing clear differences in amplitude. Other than synaptic density, all conditions are conform baseline***

Appendix II: Contour Plots

When the contour plots that are the result of placing the simulated synaptic input at individual locations are compared to those that result from input at a single location, two differences are visible. The first is the fact that for a neuron orientation of 0° the two main sources of transmembrane current (i.e. the synaptic input and the return current at the somas) appear not to be positioned in vertical alignment. Especially when compared to the plot that results from neurons at 0° and 45° angles, the positions of the sources is not as expected (i.e. one would expect the synaptic source to be near the middle of the electrode array and the return current source to be positioned underneath it).

The second difference is the fact that in the plots that represent the potentials at N_2 for the synapse specific locations seem to have extra sources of return current. That is, the plots show an extra source that is of opposite polarity compared to the one due to the excitatory synaptic input. This source, however, is believed to be a remnant of the synaptic activity at peak P_1, since both the polarity and the location of this extra source correspond to the latter.

Equal positions for both types of synaptic input

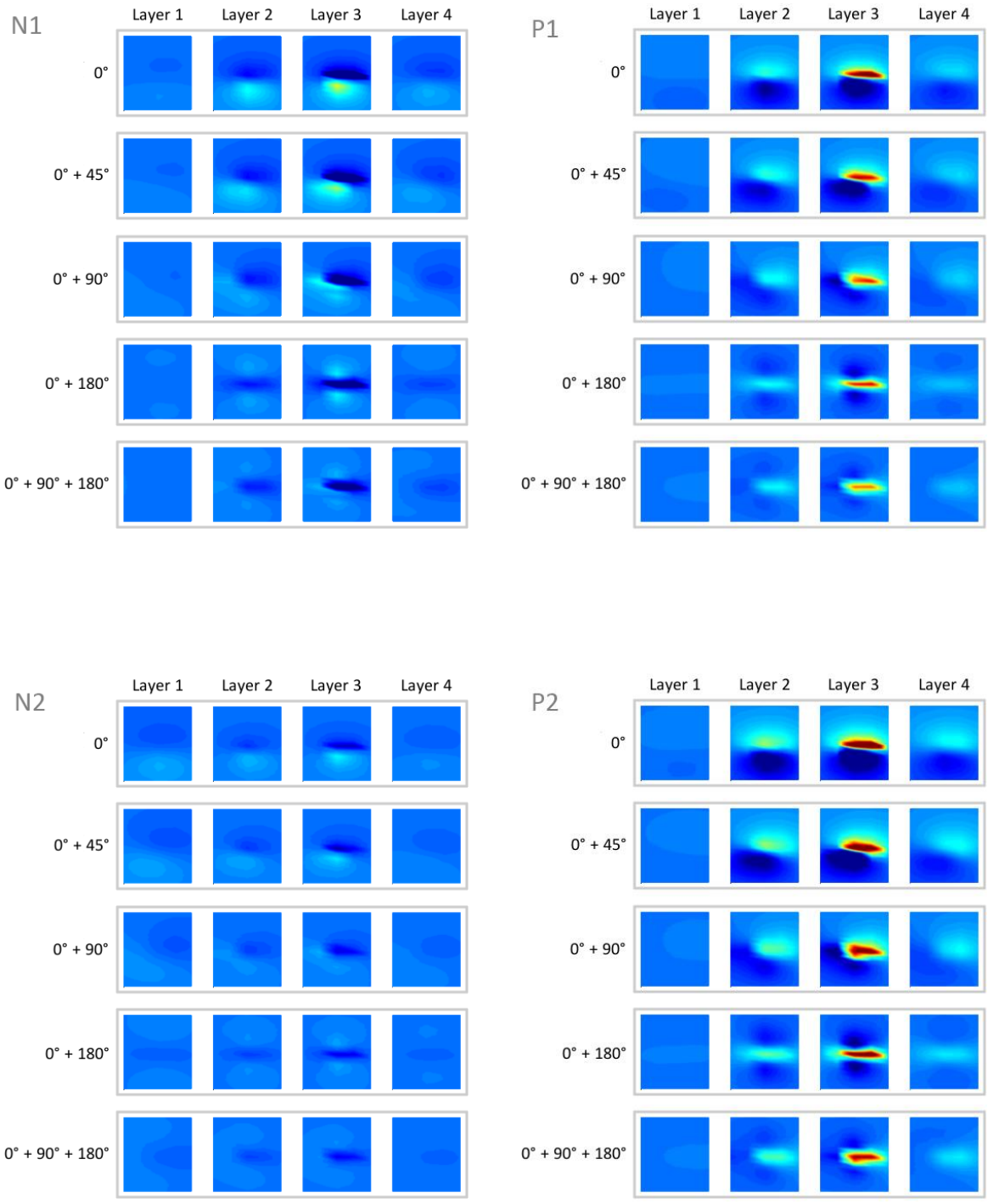

Specific locations for both types of synaptic input

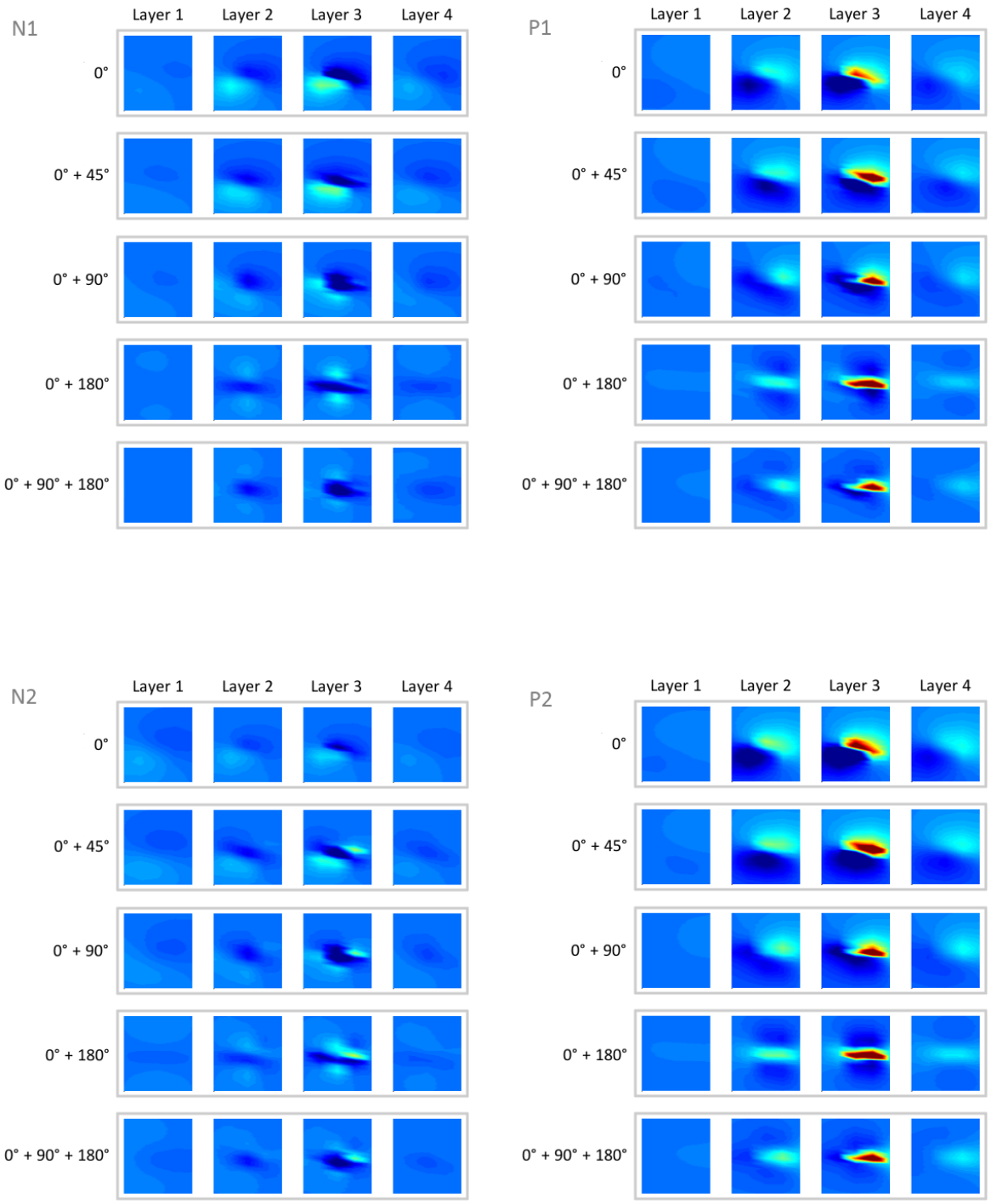

References

Bevan, M.D., Magill, P.J., Terman, D., Bolam, J.P., Wilson, C.J. (2002). Move to the rhythm: oscillations in the subthalamic nucleus–external globus pallidus network. *TRENDS in Neurosciences*. Vol.25 No.10

Brown, P. (2003). Oscillatory Nature of Human Basal Ganglia Activity: Relationship to the Pathophysiology of Parkinson's Disease. *Movement Disorders*, Vol. 18, No. 4, 2003, pp. 357–363

Brown, P. (2007). Abnormal oscillatory synchronisation in the motor system leads to impaired movement. Current Opinion in Neurobiology, 17:656–664

Butson, C.R., McIntyre, C.C. (2005). Tissue and electrode capacitance reduce neural activation volumes during deep brain stimulation. *Clinical Neurophysiology*, 116 2490–2500

Buzsáki, G., Anastassiou, C. a, & Koch, C. (2012). The origin of extracellular fields and currents--EEG, ECoG, LFP and spikes. *Nature reviews. Neuroscience*, *13*(6), 407–20. doi:10.1038/nrn3241

Carnevale, N.T., Hines, M.L. (2006). The NEURON Book. *Cambridge, UK: Cambridge University Press*

Chen, C. C., Pogosyan, A., Zrinzo, L. U., Tisch, S., Limousin, P., Ashkan, K., Yousry, T., et al. (2006). Intra-operative recordings of local field potentials can help localize the subthalamic nucleus in Parkinson's disease surgery. Experimental neurology, 198(1), 214–21. doi:10.1016/j.expneurol.2005.11.019

Clarke, N.P., Bolam, J.P. (1998). Distribution of Glutamate Receptor Subunits at Neurochemically Characterized Synapses in the Entopeduncular Nucleus and Subthalamic Nucleus of the Rat. *Journal of Comparative Neurology*, 397:403–420

Davie, C. a. (2008). A review of Parkinson's disease. *British medical bulletin*, *86*, 109–27. doi:10.1093/bmb/ldn013

Destexhe, A. et al (1998). Kynetic Models of Synaptic Transmission. Methods of Neuronal Modelling (2nd edition), MIT Press, Cambridge, MA, pp. 1-25Dorsey, E. R., Constantinescu, R., Thompson, J. P., Biglan, K. M., Holloway, R. G., Kieburtz, K., Marshall, F. J., et al. (2007). Projected number of people with Parkinson disease in the most populous nations, 2005 through 2030. *Neurology*, *68*(5), 384–6. doi:10.1212/01.wnl.0000247740.47667.03

Gillies, A., Willshaw, D. (2006). Membrane Channel Interactions Underlying Rat Subthalamic Projection Neuron Rhythmic and Bursting Activity. *Journal of Neurophysiology* 95: 2352–2365

Gillies, A., Sterratt, D. (2012). A NEURON Programming Tutorial. *http://www.anc.ed.ac.uk/school/neuron/*

Götz, T., Kraushaar, U., Geiger, J., Lübke, J., Berger, T., Jonas, P. (1997). Functional Properties of AMPA and NMDA Receptors Expressed in Identified Types of Basal Ganglia Neurons, *Journal of Neuroscience*, 17(1):204–215

Hamani, C., Saint-Cyr, J. a, Fraser, J., Kaplitt, M., & Lozano, A. M. (2004). The subthalamic nucleus in the context of movement disorders. *Brain : a journal of neurology*, *127*(Pt 1), 4–20. doi:10.1093/brain/awh029

Hammond, C., Bergman, H., & Brown, P. (2007). Pathological synchronization in Parkinson's disease: networks, models and treatments. *Trends in neurosciences*, *30*(7), 357–64. doi:10.1016/j.tins.2007.05.004

Hardman, C.D., Henderson, J.M., Finkelstein, D.I., Horne, M.K., Paxinos, G., Halliday, G.M. (2002). Comparison of the basal ganglia in rats, marmosets, macaques, baboons, and humans: volume and neuronal number for the output, internal relay, and striatal modulating nuclei. *Journal of Comparative Neurology*. 445(3):238-55.

Hines, M. (1993). NEURON A program for simulation of nerve equations. *Neural Systems: Analysis and Modeling.* Kluwer Academic Publishers, Norwell, MA, pp 127-136.

Holt, G., Koch, C. (1999). Electrical interactions via the extracellular potential near cell bodies. *J Comput Neurosci*. 1999 Mar-Apr;6(2):169-84.

Jankovic, J. (2008). Parkinson's disease: clinical features and diagnosis. *Journal of neurology, neurosurgery, and psychiatry*, *79*(4), 368–76. doi:10.1136/jnnp.2007.131045

Joël, D., Weiner, I. (1997). The connections of the primate subthalamic nucleus: indirect pathways and the open-interconnected scheme of basal ganlia-thalamocortical circuitry. *Brain Res Brain Res Rev*; 23: 62-78.

Kajikawa, Y., Schroeder, C. (2011). How local is the local field potential? *Neuron.* 2011 Dec 8;72(5):847-58. doi: 10.1016/j.neuron.2011.09.029.

Lees, A.J. Unresolved issues relating to the shaking palsy on the celebration of James Parkinson's 250th birthday. *Mov Disord. Sep 22, Suppl 17*:S327-34. doi: 10.1002/mds.21684.

Lévesque, J., Parent, A. (2005). GABAergic Interneurons in Human Subthalamic Nucleus. *Movement Disorders*. Vol. 20, No. 5, 2005, pp. 574–584

Lindén, H., Tetzlaff, T., Potjans, T.C., Pettersen, K.H., Grün, S., Diesmann, M., Einevoll, G.T. (2011). Modeling the Spatial Reach of the LFP. *Neuron*. 2011 Dec 8; 72, 859–872. doi: 10.1016/j.neuron.2011.11.006.

Magill, P.J. et al (2004). Synchronous unit activity and local field potentials evoked in the subthalamic nucleus by cortical stimulation. *Journal of neurophysiology*, 92(2), pp.700–14

Malmivuo, J., Plonsey, R. (1995). Chapter 3 – Subthreshold membrane phenomena. *Bioelectromagnetism - Principles and Applications of Bioelectric and Biomagnetic Fields*, Oxford University Press, New York

Marani, E., Heida, T., Lakke, E.A.J.F., Usunoff, K.G. (2008). The Subthalamic Nucleus – Part I: Development, Cytology, Topography and Connections, *Springer*, ISBN 978-3-540-79459-2

Martens, H.C.F., Toader, E., Decré, M.M.J., Anderson, D.J., Vetter, R., Kipke, D.R., Baker, K.B., Johnson, M.D., Vitek, J.L. (2010). Spatial steering of deep brain stimulation volumes using a novel lead design. Clinical Neurophysiology; 122 558–566

Mouradian MM, Heuser IJ, Baronti, F. et. al. (1990). Modification of central dopmenergic mechanism by continous L-DOPA therapy for advanced parkinson's disease. *Annual neurology*; 27:18-23

Pahwa, R., Lyons, K.E., (2009). Levodopa-related wearing-off in Parkinson's disease: identification and management. *Current Medical Research and Opinion*, vol. 25, NO. 4, 2009, 841–849

Parent, A., & Hazrati, L. (1995). REVIEWS Functional anatomy of the basal ganglia . II . The place of subthalamic nucleus and external pallidum in basal ganglia circuitry, *20*, 128–154.

Pettersen, K. H., Hagen, E., & Einevoll, G. T. (2008). Estimation of population firing rates and current source densities from laminar electrode recordings. *Journal of computational neuroscience*, *24*(3), 291–313. doi:10.1007/s10827-007-0056-4

Pettersen, K. H., Lindén, H., Dale, A. M., & Einevoll, G. T. (2010). Extracellular spikes and current-source density Revised chapter to appear in *Handbook of Neural Activity Measurement*, edited by Romain Brette and Alain Destexhe.

Ranck, J.B. (1964). Specific Impedance of Rabbit Cerebral Cortex. *Experimental Neurology* 7, 144-152

Rezai, A. R., Kopell, B. H., Gross, R. E., Vitek, J. L., Sharan, A. D., Limousin, P., & Benabid, A.-L. (2006). Deep brain stimulation for Parkinson's disease: surgical issues. Movement disorders : official journal of the Movement Disorder Society, 21 Suppl 1, S197–218. doi:10.1002/mds.20956

Sato, F., Parent, M., Levesque, M., & Parent, a. (2000). Axonal branching pattern of neurons of the subthalamic nucleus in primates. *The Journal of comparative neurology*, *424*(1), 142–52. Retrieved from http://www.ncbi.nlm.nih.gov/pubmed/10888744

Stocchi, F. (2006). The levodopa wearing-off phenomenon in Parkinson's disease: pharmacokinetic considerations. *Expert Opinion on Pharmacotherapy*. 7:10, 1399-1407. doi:10.1517/14656566.7.10.1399

The Deep-Brain Stimulation For Parkinson's Disease Study Group. (2001). Deep-Brain Stimulation Of The Subthalamic Nucleus Or The Pars Interna Of The Globus Pallidus In Parkinson's Disease. *The New England Journal Of Medicine*. Vol. 345, No. 13.

U.S. Department of Health and Human Services. (2006). FDA approves implanted brain stimulator to control tremors.

Van Dijk, K. (2012). Source Localization of Brain Activity, master thesis at the University of Twente, BSS-12-14.

Temel, Y., Kessels, A., Tan, S., Topdag, A., Boon, P., Visser-Vandewalle, V. (2006). Behavioural changes after bilateral subthalamic stimulation in advanced Parkinson disease: a systematic review. *Parkinsonism Relat Disord.* 12(5):265-72.